THE NATURE OF THE PRIMARY PHOTOCHEMICAL EVENTS IN RHODOPSIN AND ISORHODOPSIN

ROBERT R. BIRGE, CORA M. EINTERZ, HENRY M. KNAPP, AND LIONEL P. MURRAY
Department of Chemistry, Carnegie Mellon University, Pittsburgh, Pennsylvania 15213

ABSTRACT The nature of the primary photochemical events in rhodopsin and isorhodopsin is studied by using low temperature actinometry, low temperature absorption spectroscopy, and intermediate neglect of differential overlap including partial single and double configuration interaction (INDO-PSDCI) molecular orbital theory. The principal goal is a better understanding of how the protein binding site influences the energetic, photochemical, and spectroscopic properties of the bound chromophore. Absolute quantum yields for the isorhodopsin (I) to bathorhodopsin (B) phototransformation are assigned at 77 K by using the rhodopsin (R) to bathorhodopsin phototransformation as an internal standard ($\Phi_{R\rightarrow B} = 0.67$). In contrast to rhodopsin photochemistry, isorhodopsin displays a wavelength dependent quantum yield for photochemical generation of bathorhodopsin at 77 K. Measurements at seven wavelengths yielded values ranging from a low of 0.089 ± 0.021 at 565 nm to a high of 0.168 ± 0.012 at 440 nm. An analysis of these data based on a variety of kinetic models suggests that the I → B phototransformation encounters a small activation barrier (~0.2 kcal mol^{-1}) associated with the 9-cis ↔ 9-trans excited-state torsional-potential surface. The 9-cis retinal chromophore in solution (EPA, 77 K) has the smallest oscillator strength relative to the other isomers: 1.17 (all-trans), 0.98 (9-cis), 1.04 (11-cis), and 1.06 (13-cis). The effect of conformation is quite different for the opsin-bound chromophores. The oscillator strength of the λ_{max} absorption band of I is observed to be anomalously large (1.11) relative to the λ_{max} absorption bands of R (0.98) and B (1.07). The wavelength-dependent photoisomerization quantum yields and the anomalous oscillator strength associated with isorhodopsin provide important information on the nature of the opsin binding site. Various models of the binding site were tested by using INDO-PSDCI molecular orbital theory to predict the oscillator strengths of R, B, and I and to calculate the barriers and energy storage associated with the photochemistry of R and I for each model. Our experimental and theoretical investigation leads to the following conclusions: (*a*) The counterion (abbreviated as CTN) is not intimately associated with the imine proton in R, B, or I. The counterion lies underneath the plane of the chromophore in R and I, and the primary chromophore-counterion electrostatic interactions involve C_{15}—CTN and C_{13}—CTN. These interactions are responsible for the anomalous oscillator strength of I relative to R and B. (*b*) The presence of a small activation barrier (~0.2 kcal mol^{-1}) in the 9-cis → 9-trans excited-state surface is associated with the location of the counterion as well as the intrinsic photophysical properties of the 9-cis chromophore. The principal difference between the 11-cis → 11-trans photoreaction surface and the 9-cis → 9-trans photoreaction surface is the lack of effective electrostatic stabilization of distorted 9 = 10 conformations due to incomplete charge polarization. (*c*) Hydrogen bonding to the imine proton, if present, does not involve the counterion. We conclude that water in the active site, or secondary interactions with the protein (not involving the CTN), are responsible. (*d*) All photochemical transformations involve one-bond photoisomerizations. This prediction is based on the observation of a very small excited state barrier for the I → B photoreaction and a negative barrier for the R → B phototransformation, coupled with the theoretical prediction that all two-bond photoisomerizations have significant S_1 barriers while one-bond photoisomerizations have small to negative S_1 barriers. (*e*) Rhodopsin is energetically stabilized relative to isorhodopsin due to both electrostatic interactions and conformational distortion, both favoring stabilization of R. The INDO-PSDCI calculations suggest that rhodopsin chromophore-CTN electrostatic interactions provide an enhanced stabilization of ~2 kcal mol^{-1} relative to I. Conformational distortion of the 9-cis chromophore-lysine system accounts for ~3 kcal mol^{-1}. (*f*) Energy storage in bathorhodopsin is ~60% conformational distortion and 40% charge separation. Our model predicts that the majority of the chromophore-protein conformational distortion energy involves interaction of the $C_{13}(—CH_3)=C_{14}—C_{15}=$N-lysine moiety with nearby (unknown) protein residues. (*g*) Strong interactions between the counterion and the chromophore in R and I will generate weak, but potentially observable charge-transfer bands in the near infrared. The key predictions are the presence of an observable charge-transfer transition at 859 nm (11,640 cm^{-1}) in I and an analogous, but slightly weaker band at 897 nm (11,150 cm^{-1}) in R. Both transitions involve the transfer of an electron from the counterion into low-lying π^* molecular orbitals.

Direct reprint requests to R. R. Birge at Department of Chemistry, Syracuse University, 108 Bowne Hall, Syracuse, New York. 13244-1200.

INTRODUCTION

Rhodopsin (R) is the light-harvesting protein in the rod outer segments of vertebrate and invertebrate photoreceptors (Birge, 1981). This protein undergoes a photobleaching sequence which is responsible for activating a complex series of reactions which ultimately generate an optic nerve impulse (Stryer, 1986). It is now accepted generally that the primary photochemical event involves an 11-cis → 11-trans photoisomerization of the protonated Schiff base retinyl chromophore (Ottolenghi, 1980; Birge, 1981). The mechanisms through which the protein influences the energetics and dynamics of the primary process have not been explained fully. For example, an 11-cis protonated Schiff base in solution photoisomerizes to the all-trans configuration in ~10 ns with a quantum yield of ~0.3 to yield a ground-state photoproduct, which is energetically more stable (Hupert et al., 1977; Becker and Freedman, 1985). Rhodopsin (11-cis) photoisomerizes to bathorhodopsin (B) (all-trans) in ~3 ps with a quantum yield of 0.67 to yield a ground state photoproduct with an increased enthalpy of ~32 kcal mol^{-1} (Cooper, 1979a; Schick et al., 1987). The protein binding site, therefore, has a dramatic influence on the dynamics, quantum yield, and energy storage associated with the chromophore photoisomerization. The present study of the spectroscopic, photochemical, and photocalorimetric properties of the artificial analog, isorhodopsin (I), seeks to provide a clearer understanding of how the protein influences these properties.

The analysis presented below is based upon the assumption that the batho product produced by photolysis of rhodopsin is identical to that produced by photolysis of isorhodopsin. Studies comparing the kinetic and spectral characteristics of the batho products from R and I on picosecond (Monger et al., 1979) and nanosecond (Kliger et al., 1984) time scales support this assumption, as does the observation of a photoequilibrium between R, I, and a red-shifted photoproduct at low temperatures (Yoshizawa and Wald, 1963). The notion of a common batho intermediate has been complicated by observations that under certain experimental conditions (excitation intensity, temperature) at least two batho products are produced after photolysis of rhodopsin (Pratt et al., 1964; Sasaki et al., 1980 a, b; Einterz et al, 1987). More recently, Kliger and coworkers (private communication) have shown that photolysis of isohodopsin also yields multiple batho photoproducts, which are similar in the kinetic and spectral behavior to those formed following photolysis of rhodopsin. The above evidence indicates that the following equilibrium pertains:

$$\text{rhodopsin (R)} \underset{h\nu}{\overset{h\nu}{\rightleftharpoons}} \text{bathorhodopsin (B)} \underset{h\nu}{\overset{h\nu}{\rightleftharpoons}} \text{isorhodopsin (I)}$$

Scheme I

where it is understood that "bathorhodopsin (B)" may represent more than one species (perhaps involving slightly different protein environments).

Isorhodopsin is an artificial analog of rhodopsin which can be generated by incorporating 9-cis retinal into opsin or generated photochemically in-situ by irradiation of rhodopsin at 77k by 580 nm light (Yoshizawa and Wald, 1963). The pigments generated by the above two methods are spectroscopically (Mao et al., 1980) and energetically (Schick et al., 1987) identical. Although isorhodopsin has a ground state enthalpy ~5 kcal mol^{-1} higher than rhodopsin, it will undergo an identical bleaching sequence to that observed for rhodopsin. The key observation for the purposes of this paper is the following: the chromophores in rhodopsin and isorhodopsin, although different cis isomers, must occupy structurally identical binding sites in order to accommodate identical photoproducts. (Our use of the adjective "identical" is not intended to exclude modest relaxation of the protein matrix that may occur to stabilize a 9-cis versus an 11-cis chromophore.) Although this important conclusion is frequently assumed to apply to a variety of other artificial pigments, isorhodopsin is unique because of the large body of spectroscopic, photochemical, and photocalorimetric data available in support of this conclusion.

Given the unique characteristics of isorhodopsin, it is surprising that this artificial pigment has not received greater experimental and theoretical attention. We will demonstrate that a detailed examination of the spectroscopic, photochemical, and photocalorimetric differences between rhodopsin and isohodopsin provides new insights into the nature of the protein binding site.

METHODS

Preparation of Rhodopsin

Purified rhodopsin rod outer segments (ROS) were prepared by using the step-wise surcrose gradient method described by Hong, et al. (1982) as modified by Schick, et al. (1987). We will refer to the ROS preparation as rhodopsin or R in the remainder of the paper. Prior to spectroscopic or photochemical study, the rhodopsin was solubilized in 67% glycerol/2% digitonin/10 mM potassium phosphate buffer at pH 7.0.

Preparation of Isorhodopsin

I was prepared at 77 K in situ by irradiation of R, or a mixture of R, I, and B at 580 nm. A 100 W Xenon lamp was used as the excitation source with wavelength selection accomplished by using a chemical filter (3 g $K_2Cr_2O_7$ in 100 cc H_2O, 10 cm path length) followed by an interference filter (580 nm, 4 nm full width half maximum [FWHM] band pass) (Schick, et al., 1987). This technique has been used by Yoshizawa and Wald (1963) and by Mao et al (1980) to generate isorhodopsin identical spectroscopically to that generated via direct incorporation of 9-cis retinal into opsin. We carried out selected experiments using isorhodopsin prepared via the latter method to determine whether the pigment so generated differed in terms of photochemical quantum yield for bathorhodopsin formation from that produced via in situ irradiation of rhodopsin. Within experimental error, no differences were observed.

Low Temperature Absorption Spectra

The low temperature (77 K) absorption spectra of all-trans, 9-, 11-, and 13-cis retinal were measured by using a liquid nitrogen dewar mounted inside the optical cavity of a Cary 17 D double-beam spectrophotometer (Varian Associates, Inc., Palo Alto, CA). Two solvent mixtures were used: EPA (ethyl ether, isopentane, ethanol; 5:2:2, vol/vol) and PMh (isopentane, methylcyclohexane; 5:1, vol/vol). Isomeric purity of the samples was verified to be >95% based on ^1H and ^{13}C nuclear magnetic resonance.

The low temperature absorption spectra of R and I were measured at 77 K in the wavelength region 450–700 nm by using a closed cycle helium cold tip (Air Products, Allentown, Pennsylvania, Displex with digital temperature controller) mounted inside the optical cavity of an EU-700 computer-controlled double-beam spectrophotometer (McPherson, Acton, Massachusetts). Because of the difficulties of verifying complete incorporation, the measurement of the I spectrum was carried out by using a rhodopsin sample photochemically converted to I (see above). Photostationary state mixtures of varying composition were used to measure the spectrum of B. These mixtures, containing various amounts of R, B, and I, were generated by using a flashlamp-pumped tunable dye laser to generate nearly monochromatic irradiation at the following wavelengths: 440, 461, 479, 498, and 520 nm (see below). The absorption spectrum of B was determined by using successive subtractions of R and I spectra by using the stationary state measurements of Suzuki and Callender (1981) and Bagley et al. (1985) to predict concentrations of R and I. The final spectrum was an average of the five spectra weighted by the inverse of the error determined by propagation of the errors in component concentrations (see Birge and Callender, 1988). Because of this weighting procedure, the final spectrum of B was defined primarily by the 440, 461, and 479 nm stationary states, because these excitation wavelengths generate the largest fractional concentrations of B.

Quantum Yields of Isorhodopsin Photoconversion

The quantum efficiency of formation of bathorhodopsin from isorhodopsin as a function of wavelength was measured by using a laser irradiated closed-cycle helium cold tip (Air Products Displex with digital temperature controller) located inside the optical cavity of a McPherson EU700 double-beam absorption spectrophometer. The spectrophotometer was computer controlled by a PDP 11/23 microcomputer, and was designed to permit isolation of the photomultiplier during laser irradiation. The optical configuration allowed for perpendicular excitation followed by measurement of the absorption spectrum without disturbing the optical configuration. R was used as an internal standard assuming a wavelength independent quantum yield for B formation of 0.67 (see Birge and Callender, 1987). Laser irradiation was provided by a Phase-R flashlamp pumped tunable dye laser modified as described by Bennett and Birge (1980). The following wavelengths were generated by using the laser dyes, dye concentrations, and solvents listed in parentheses following the wavelength in nanometers: 440 (coumarin 440, 3×10^{-4} M, ethanol), 461 (coumarin 460, 1.5×10^{-4} M, methanol), 479 (LD490, 1×10^{-4} M, ethanol), 498 (coumarin 503:307/1:1,1×10^{-4} M), 520 (coumarin 522, 2×10^{-4} M, ethanol), 541 (coumarin 540:153/1:1,1×10^{-4} M, methanol), and 565 (rhodamine 560:110/1:1,5×10^{-5} M, methanol). A sample of R was irradiated at each of the above wavelengths and the total absorption spectrum measured after each sequence of 50 laser pulses. This sequence was repeated for 10–20 repetitions and the total spectrum, as well as the total number of photons per individual laser pulse, stored on disk for each repetition. The number of photons per pulse was measured by using a calibrated Joule meter after the procedures described by Schick et al. (1987). After this sequence, the sample was irradiated by using a 100W Xenon lamp (Oriel Corporation, Stratford, Connecticut) filtered through a chemical filter (3 g $K_2Cr_2O_7$ in 100 cc H_2O, 10 cm path length) followed by an interference filter (580 nm, 4 nm FWHM band pass) to convert the reaction mixture to pure I (see above). The experimental sequence was then repeated using laser irradiation at the same wavelength. All of the laser excitation photochemistry was conducted by using a defocussed laser beam in order to irradiate, as evenly as possible, the entire cell, and the intensity was adjusted to assure that <1% of the starting material was photoreacted during the 50 pulse sequence. The fraction of molecules reacted was calculated by deconvoluting the absorption spectra into contributions of reactant and product and assuming rigorous Beer's law behavior. The experiment was discontinued when 6% of the starting material was reacted (the remaining data sets were discarded). The quantum yield for the I → B reaction was determined by using the following approach based on the pulsed laser absorption algorithms reviewed by Birge (1983).

The number of molecules promoted into the excited state, N^*, is given by,

$$N^* = N_{\text{laser}} \times A_\lambda, \tag{1}$$

where N_{laser} is the number of photons entering the reaction cell during the excitation sequence and A_λ is the wavelength-dependent absorption parameter,

$$A_\lambda = 1 - \exp(-\sigma_\lambda CL), \tag{2}$$

where C is the concentration of the reactant, L is the path length of the cell, and σ_λ is the one-photon cross section. The one-photon cross section is related to a more convenient experimental observable by the equation,

$$\sigma_\lambda = 1{,}000\ (\ln 10) \times \epsilon_\lambda = (3.8235 \times 10^{-21})\ \epsilon_\lambda, \tag{3}$$

where ϵ_λ is the molar absorptivity at wavelength λ. This parameter is measured as part of the experimental procedure at the start of each reaction sequence (in fact, the entire spectrum from 300–700 nm is measured). (For the purposes of this derivation, we assume that the only absorbing species in the solution is the reactant. As explained below, however, least squares regression techniques will be used to correct for the absorption of irradiation by product.) The number of excited state species that convert to form the primary photoproduct, N_{prod}, is given by,

$$N_{\text{prod}} = \Phi_{\text{isom}} \times N^* = \Phi_{\text{isom}} \times N_{\text{laser}} \times A_\lambda, \tag{4}$$

where Φ_{isom} is the quantum yield for the photochemical process. The quantum yield of formation of bathorhodopsin from isorhodopsin, $\Phi_{I \to B}$, can therefore be calculated by measuring,

$$\Phi_{I \to B} = \left(\frac{N_{\text{prod}}^{I \to B}}{N_{\text{laser}} \times A_\lambda^I} \right), \tag{5}$$

where the ratio shown in brackets can be obtained, in principle, from deconvolution of the reaction mixture spectra along with accurate actinometry to measure the number of photons entering the cell. The former measurement is much easier to perform than the latter measurement, and it is thus useful to use an internal standard to calibrate the laser flux relative to the joule meter response. An equation analogous to that of Eq. 5 can be written for R,

$$\Phi_{R \to B} = \left(\frac{N_{\text{prod}}^{R \to B}}{N_{\text{laser}} \times A_\lambda^R} \right). \tag{6}$$

The number of photons in the laser pulse entering the sample cell is given by,

$$N_{\text{laser}} = \kappa \times (5.03402 \times 10^{12}) \cdot E(\text{mj/pulse}) \cdot \lambda(\text{nm}) \tag{7}$$

where E is the energy measured by using the Joule meter, λ is the wavelength of the laser excitation beam and κ is the distribution factor which defines the amount of laser light entering the cell divided by the

amount of light directed into the Joule meter. Because the laser beam is divided by an achromatic beam splitter and defocussed into the cell using an achromatic beam expander and a fixed aperture, we can be confident that κ is not a wavelength dependent variable. An accurate determination of κ, however, is difficult and would represent the major source of error in determining the absolute quantum yield. An alternative is to use R as an internal standard which eliminates the need to specify κ. The following equation was used to determine the I → B quantum yield as a function of laser wavelength,

$$\Phi_{I\to B} = \Phi_{R\to B}\left(\frac{N_{prod}^{I\to B}\cdot \Sigma E_{R\to B}\cdot \lambda_{R\to B}\cdot A_{\lambda}^{R}}{N_{prod}^{R\to B}\cdot \Sigma E_{I\to B}\cdot \lambda_{I\to B}\cdot A_{\lambda}^{I}}\right) \quad (8)$$

where $\Sigma E_{I\to B}$ is the sum of the laser pulse energies used to irradiate I (sum of the 50 laser pulses), $\lambda_{I\to B}$ is the wavelength of the laser excitation, and the remaining terms are defined analogously. All reported quantum yields assume $\Phi_{R\to B}$ is equal to 0.67 (see Birge and Callender, 1988, for experimental verification of the wavelength independence of $\Phi_{R\to B}$). Eq. 8 was used to determine $\Phi_{I\to B}$ for each 50 pulse sequence, and the data were fit to a quadratic equation with the independent variable assigned to the total number of laser excitation photons. The leading term represents $\Phi_{I\to B}$ under the desired initial conditions (pure I, negligble excitation energy). A quadratic fit to the data was chosen in preference to a linear fit because our choice of a 6% reaction cut-off (see above) does not prevent slight contamination of the measurement via formation of R. This problem will induce a quadratic dependence of $\Phi_{I\to B}$ (measured) relative to the total number of laser excitation photons absorbed by the reaction mixture. Although our use of a quadratic function had no significant effect on the values reported for $\Phi_{I\to B}$, we anticipate that the calculated standard deviations in $\Phi_{I\to B}$ based on the quadratic fits are more realistic than those predicted based on the linear fits.

Oscillator Strengths of the λ_{max} Absorption Bands

The low temperature absorption spectra have well defined λ_{max} absorption bands in the wavelength regions 450–700 nm. At wavelengths to the blue of 450 nm, however, high energy transitions start to contribute to the absorption spectra. This problem prompted our use of the log-normal fitting procedures proposed by Metzler and Harris (1978). These investigators have shown that the band shapes of many visual chromophores and visual pigments can be fit to good precision by using the following log-normal distribution function,

$$\epsilon(\nu) = \epsilon_0 \exp -\left\{\frac{\ln 2}{(\ln \rho)^2}\left[\ln\left(\frac{(\nu-\nu_0)(\rho^2-1)}{W\rho}+1\right)\right]^2\right\},$$

$$\nu > \nu_0 - [W\rho/(\rho^2-1)]; \quad (9a)$$

$$\epsilon(\nu) = 0, \quad \nu \le \nu_0 - [W\rho/(\rho^2-1)], \quad (9b)$$

where $\epsilon(\nu)$ is the molar absorptivity at wave number ν, ν_0 is the wave number at maximum absorptivity, ϵ_0 is the molar absorptivity at ν_0, W is the fwhm in wave numbers and ρ is the skewness. The skewness is a dimensionless parameter, which is an indirect measure of the distribution of vibronic activity into higher vibrational modes due to Franck-Condon activity. One can demonstrate using wave packet propagation theory that the log-normal distribution is an accurate representation of an electronic band shape provided a single vibrational mode dominates the Frank-Condon progression and inhomogeneous broadening is severe.

The oscillator strength of a one-photon electronic transition can be calculated based on a log-normal intensity distribution,

$$f = \frac{10^3 \ln 10\, mc^2}{N_a \pi e^2}\int_0^{\infty}\epsilon(\nu)d\nu \quad (10)$$

$$f = 4.319\times 10^{-9}\sqrt{\pi/\ln 2}\times \epsilon_0 W\left\{\frac{\rho(\ln\rho)}{(\rho^2-1)}\exp\left[\frac{(\ln\rho)^2}{4\ln 2}\right]\right\} \quad (11)$$

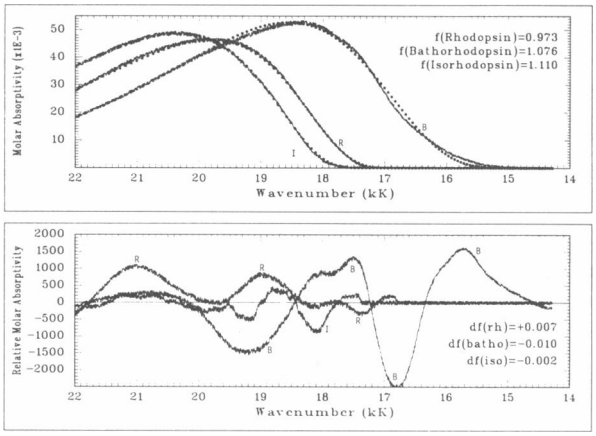

FIGURE 1 Absorption spectra of rhodopsin, bathorhodopsin, and isorhodopsin solubilized in 67% glycerol/2% digitonin/10 mM potassium phosphate buffer (pH 7.0) at 77 K (*top*). The curves generated by using log-normal regression are shown as dots superimposed on the individual spectra, and the difference spectra (observed-minus-calculated) are expanded in the bottom graph. Oscillator strengths calculated from the log-normal fits (Eq. 11) are listed in the top graph, and the corrections to the calculated oscillator strengths obtained by integrating under the difference curves are listed in the bottom graph. The log-normal value plus the correction integral is used as the experimental measurement of the oscillator strength (see Table I and text).

TABLE I
SPECTROSCOPIC PROPERTIES OF RHODOPSIN, BATHORHODOPSIN AND ISORHODOPSIN AT 77 K

Measurement	Rhodopsin	Bathorhodopsin	Isorhodopsin
ϵ (440 nm)*	23.9	12.2	36.2
ϵ (461 nm)	31.6	21.0	39.7
ϵ (479 nm)	40.9	30.0	46.9
ϵ (498 nm)	45.9	39.7	47.9
ϵ (520 nm)	43.7	47.8	36.2
ϵ (541 nm)	28.2	52.4	15.3
ϵ (565 nm)	6.1	46.4	0.6
λ_{max} (nm)	505	543	492
$\epsilon(\lambda_{max})$	46.4	52.5	48.6
f(λ_{max} band)‡	0.98	1.07	1.11
Log-normal fit§			
ν_{max} (cm^{-1})	19,805(±4)	18,554(±12)	20,332(±4)
$\epsilon(\nu_{max})$	46.93	52.24	48.55
error in $\epsilon(\nu_{max})$	±0.06	±0.19	±0.06
$\Delta\nu_{FWHM}$ (cm^{-1})	4,245(±17)	4,264(±26)	4,562(±24)
ρ (skewness)	1.855	1.600	1.936
error in ρ (skewness)	±0.011	±0.018	±0.013
r^2	0.9998	0.9976	0.9999

*Molar absorptivities, ϵ, are listed in M^{-1} cm^{-1} × 10^{-3}. Errors are estimated to be ±5% or ±0.2, whichever is larger.
‡Oscillator strength obtained by using log-normal fit (Eq. 11) and subsequently applying correction integral as described in text.
§Parameters listed were obtained from log-normal fit of absorption spectra from 450–700 nm.

TABLE II

OBSERVED AND CALCULATED QUANTUM YIELDS AS A FUNCTION OF LASER EXCITATION WAVELENGTH FOR THE PHOTOCHEMICAL FORMATION OF BATHORHODOPSIN FROM ISORHODOPSIN AT 77 K

λ_{exc}(nm)*	$\Phi_{I\rightarrow B}^{obs}$‡	$\Phi_{I\rightarrow B}^{calc}$ (model B)§	$\Phi_{I\rightarrow B}^{calc}$ (model C)‖
440	0.168 ± 0.012	0.175	0.164
461	0.157 ± 0.017	0.168	0.164
479	0.165 ± 0.009	0.160	0.163
498	0.163 ± 0.014	0.150	0.160
520	0.142 ± 0.008	0.136	0.144
541	0.108 ± 0.012	0.118	0.107
565	0.089 ± 0.021	0.088	0.089

*Laser excitation wavelength in nanometers.

‡Quantum yield measured for the isorhodopsin → bathorhodopsin transition at 77 K. Values are listed as absolute yields, but were measured by using rhodopsin as an internal standard with an assigned quantum yield (R → B) of 0.67 (see Eq. 8).

§Quantum yield calculated for the isorhodopsin → bathorhodopsin transition at 77 K based on model B (see text).

‖Quantum yield calculated for the isorhodopsin → bathorhodopsin transition at 77 K based on model C (see text).

Subsequent equations assume that ϵ_0 is in M^{-1} cm^{-1} and that W is in cm^{-1}. Eq. 11 reduces to a much simpler form for a purely Gaussian distribution ($\rho \rightarrow 1$):

$$f = 4.319 \times 10^{-9} \sqrt{\pi/\ln 2} \times \epsilon_0 W(1/2) \quad (\rho \rightarrow 1) \qquad (12)$$

$$f = 4.597 \times 10^{-9} \epsilon_0 W \quad (\rho \rightarrow 1), \qquad (13)$$

where the term in brackets in Eq. 11 is evaluated by using L'Hopital's rule for $\rho \rightarrow 1$.

The advantage of using Eq. 11 for the present oscillator strength assignments is associated with the ability of the log-normal distribution to represent accurately the higher energy regions of electronic bands (Metzler and Harris, 1978, Birge et al., 1982). By fitting the lower energy regions of the R, B, and I absorption spectra to log-normal distributions, the interference associated with higher energy absorption bands can be circumvented.

Two electronic transitions contribute to the λ_{max} absorption bands: "$^1A_g^{*-}$" ← S_0 and "$^1B_u^{*+}$" ← S_0 (Birge et al., 1985). Although a majority of the intensity of the λ_{max} band is associated with the strongly allowed "$^1B_u^{*+}$" ← S_0 transition, inclusion of the "$^1A_g^{*-}$" ← S_0 transition is necessary to model the oscillator strength accurately using molecular orbital theory. All of the calculations of oscillator strength presented in this paper included contributions from both transitions.

Molecular Orbital Calculations

The all-valence electron INDO-PSDCI procedures described by Birge and Hubbard (1980, 1981) were used. All single excitations below 15 eV and all double excitations below 20 eV were included in the CI Hamiltonian for the excited state calculations. These energy constraints generated a CI Hamiltonian containing ~300 single and ~700 double excitations for the model pigment systems investigated here. Transitions from the counterion to the chromophore were explicitly excluded from the CI Hamiltonian in a number of calculations to limit the final state distribution. These charge transfer states result in low-lying, optically forbidden (or very weak) transitions which do not mix with the chromophore valence transitions (LeClercq and Sandorfy, 1981). Exclusion of charge transfer states does not diminish the accuracy of the valence state calculations, but saves considerable computation time given the size of the CI matrix. Ground state calculations used standard INDO procedures (Pople et al, 1967).

RESULTS AND DISCUSSION

The absorption spectra of R, B, and I at 77 K were analyzed by using a log-normal fit. The results are presented Fig. 1 and Table I. Absolute quantum yield data as a function of excitation wavelength associated with phototransformation of isorhodopsin to bathorhodopsin are given in Table II and compared with theoretical models (see below) in Table II and Fig. 2. These results represent the major experimental components of this study, and as noted below, indicate that I has two anomalous photophysical properties that provide insight into the nature of the opsin protein binding site.

The explanation of the origin and photophysical significance of a wavelength dependence in the I → B quantum yield represents one of the principal goals of this paper. This interesting and unique characteristic of I was first observed by Hurley et al. (1977), but subsequent investigations of I photochemistry either ignored or contradicted their observation. We reinvestigated this issue in the course of carrying out photocalorimetric investigations of energy storage in the primary events of R and I (Schick et al., 1987). In particular, preliminary measurements of energy storage in I based on a fixed quantum yield, $\Phi_{I\rightarrow B}$, of 0.1

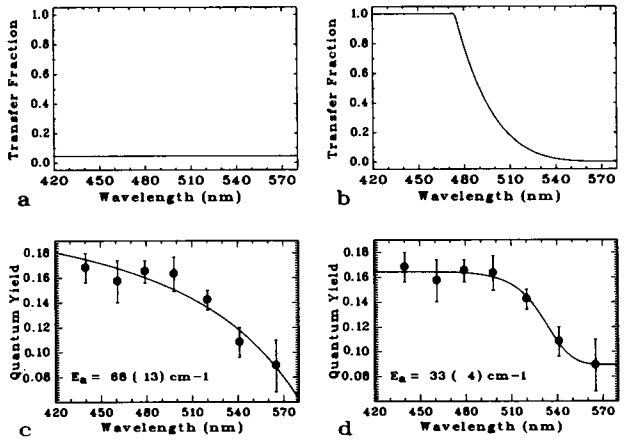

FIGURE 2 Two theoretical models describing the wavelength dependence of the isorhodopsin → bathorhodopsin quantum yield are compared. The transfer fraction and quantum yield predictions for model B are shown in graphs a and c, respectively. Graphs b and d present the results for model C.

(Suzuki and Callender, 1981) yielded wavelength-dependent primary event enthalpies of storage. This result was contrary to the wavelength independence observed for R, and while complicated mechanisms could be proposed to explain such an observation, none appeared logical based on currently accepted mechanisms of energy storage (Schick et al., 1987). The most logical explanation was that our assumption of a wavelength independence in $\Phi_{I\rightarrow B}$ was not correct. Direct measurements of $\Phi_{I\rightarrow B}$ at seven wavelengths after the procedures described in Methods yielded the values listed in Table II. These data, when incorporated into the photocalorimetry analysis, generated wavelength independent energy storage enthalpies for the primary event in I (Schick et al., 1987). The observation of a wavelength and temperature dependent quantum yield for the I → B phototransformation prompted a reexamination of the other quantum yields associated with the photochemical triad (Birge and Callender, 1988):

$$\text{rhodopsin (R)} \underset{\Phi_2}{\overset{\Phi_1}{\rightleftharpoons}} \text{bathorhodopsin (B)}$$

$$\underset{\Phi_4(\lambda,\, T)}{\overset{\Phi_3}{\rightleftharpoons}} \text{isorhodopsin (I)} \quad (14)$$

The results of the latter study indicate that only $\Phi_{I\rightarrow B}$ (hereafter abbreviated Φ_4) displays wavelength or temperature dependence. The remaining quantum yields are independent of both variables within the error ranges specified: $\Phi_1 = 0.67 \pm 0.02$, $\Phi_2 = 0.49 \pm 0.03$, $\Phi_3 = 0.076 \pm 0.006$ (Birge and Callendar, 1988).

Before analyzing the unusual photochemical behavior of I, we note that a second anomaly was uncovered in the course of this investigation. The accurate measurement of Φ_4 requires a careful measurement of the absorption spectra of R, B, and I under identical solvent and temperature conditions. The results, shown in Fig. 1, indicate that I has the largest oscillator strength of the three proteins, an observation contrary to that predicted for a 9-cis chromophore relative to the all-trans and 11-cis visual chromophores in solution (Schaffer et al. 1974, Honig et al. 1980).

We will demonstrate below that the above two anomalies involving the spectroscopic and photochemcial properties of I are related and that an analysis of the molecular origins provides new perspectives on the opsin binding site.

Primary Quantum Yields of Isorhodopsin Photochemistry

The observed quantum yields for I → B photoconversion at 77 K are listed in Table II and graphed in Fig. 2. It is interesting to compare these data with the quantum yields associated with the phototriad (R ↔ B ↔ I) at ambient temperature (Fig. 3).

At ambient temperature, $\Phi_4 = 0.22 \pm 0.03$ and displays no wavelength dependence within the error range specified

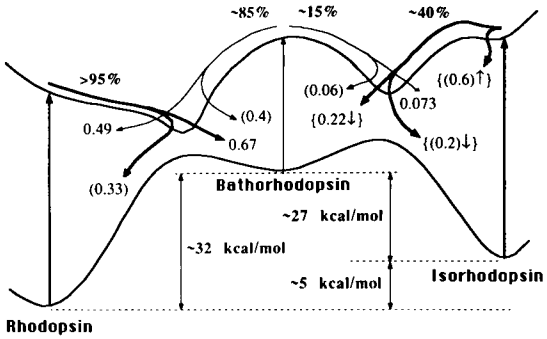

FIGURE 3 Schematic representation of the ground and first excited singlet state surfaces connecting rhodopsin, bathorhodopsin and isorhodopsin using a linearized reaction coordinate. The shapes of the ground and excited surfaces are based on INDO-PSDCI calculations (see text). Ground state enthalpies are taken from the experimental measurements of Cooper (1979b) and Schick et al. (1987). Absolute quantum yield of photoisomerization are displayed at the tips of the arrows indicating the processes (Birge and Callender, 1987). Values given in parentheses (●) are predicted by using semiempirical molecular dynamics theory to calculate the reverse/forward yield ratios and multiplying these values by the experimental forward yields (shown without parentheses). Values listed in brackets {●} are ambient temperature quantum yields which display temperature dependence. The arrows indicate the effect that lowering the temperature will have on these values, e.g., {0.22↓} indicates that at lower temperatures, the quantum yield will be lower than 0.22

(Hurley et al., 1977). This behavior is in contrast to the wavelength dependence observed at 77 K (Table II). The picosecond experiments of Monger et al. (1979) indicate that both R and I form B in ~3 ps. This observation indicates that both photoreactants (R and I) have highly efficient reaction pathways (low to negative barriers to photoisomerization and efficient coupling into the ground state surface). Based on the molecular dynamics calculations of Birge and Hubbard (1980, 1981), a 3 ps photoreaction time indicates that any barrier must be <1 kcal mol^{-1} and is probably <0.5 kcal mol^{-1}. The observation that the quantum yield decreases with decreasing temperature, but increases with increasing excitation energy at 77 K, suggests that there is a small but nonnegligible barrier for 9-cis → 9-trans photoisomerization in the excited state.

In the following paragraphs we will attempt to calculate the barrier for 9-cis → 9-trans photoisomerization in the excited state. We will demonstrate that both simple Arrhenius models as well as more complicated wavelength dependent models lead to similar conclusions concerning the magnitude of the barrier (or "effective barrier" if inhomogeneity generates a distribution of barriers).

Arrhenius activation energy (model A). We initiate our analysis by invoking the following assumption,

$$\Phi_{isom} \propto \frac{k_{isom}}{(k_{isom} + k_{ic})} \quad (15)$$

where k_{isom} represents the rate of photoisomerization and k_{ic} represents the rate of direct internal conversion back to the ground state. We assume further that k_{ic} is wavelength

and temperature independent, an assumption that is realistic only for systems where internal conversion is extremely rapid (radiative processes are not competitive) and only one reaction path leads to photoisomerized product. Experimental studies suggest that Eq. 15 is a reliable approximation for studying polyene photochemistry (Saltiel et al. 1972, Waddell and Chihara, 1981). The Arrhenius approximation gives,

$$k_{isom} = A_{isom} \cdot \exp(-E_a/RT), \quad (16)$$

where A_{isom} is an unknown pre-exponential factor (assumed constant), E_a is the activation barrier for photoisomerization, R is the gas constant and T is the absolute temperature. It is thus possible to equate the quantum yield of photoisomerization directly with the activation energy,

$$\Phi_{isom} = \zeta \cdot \exp(-E_a/RT), \quad (17)$$

where ζ is a constant $[= A_{isom}/(k_{isom} + k_{ic})]$ which is assumed to be wavelength and temperature independent (see above). Assignment of ζ is both difficult and unnecessary provided Φ_{isom} data are available as a function of temperature. I data are available at ambient (300 K) and liquid nitrogen (77 K) temperatures, and a direct calculation of E_a is possible:

$$E_a(\text{cm}^{-1}) = 72.9 \cdot \ln\left(\frac{\Phi_4^{300K}}{\Phi_4^{77K}}\right) \quad (18)$$

Assignment of E_a by using Eq. 18 is complicated in the present case by the wavelength dependence observed in Φ_4^{77K} (see Table II). Nonetheless, if we simply take an average of the available data and fold the wavelength dependence into the error range, we get $\Phi_4^{77K} = 0.12 \pm 0.06$ and calculate $E_a = 50 \pm 35\ \text{cm}^{-1} = 0.14 \pm 0.10$ kcal mol^{-1}. This value is likely to represent a lower limit since arguments to be presented below suggest that the wavelength dependence is best interpreted as a partitioning of excess vibrational energy into torsional kinetic energy. Hence, the actual barrier should be calculated in reference to the long wavelength value of Φ_4^{77K} (565 nm) = 0.089 ± 0.021. Substitution of the latter quantum yield into Eq. 18 yields $E_a = 70 \pm 18\ \text{cm}^{-1} = 0.20 \pm 0.05$ kcal mol^{-1} (see Table III).

The approximate nature of the above calculation of activation energy should be emphasized. First, the observation of a wavelength dependence at low temperature, and the absence of a wavelength dependence at ambient temperature, indicates that I photochemistry does not follow rigorous Arrhenius-type behavior. Second, a full temperature dependence study of Φ_4 is difficult to justify given the experimental difficulties of assigning very small changes in quantum yield. (A decrease of 220 K induces a decrease in Φ_4 of ~0.1. Thus, the quantum yield measurements must be evaluated over a large temperature range in order to observe changes that are not masked by experimental error. The latter observation should not preclude the industrious researcher from attempting a study of this kind. However, it would represent a major investigation unto itself, and is beyond the scope of this study.) Accordingly, we prefer to view the Arrhenius approximation results as illustrative, rather than quantitative. The important point is not that the results are independently important, but rather that the close numerical agreement of the Arrhenius calculation with the wavelength-dependent simulation results provides a perspective on the legitimacy of our analysis.

Wavelength dependent simulations of the quantum yield (models B and C). The above model provides insight into the activation energy, but fails to explain the origin of the wavelength dependence of the low temperature quantum yield. We present here two models of the wavelength dependence, both of which simulate within experimental error, the observed data (see Fig. 2). Both

TABLE III

DETERMINATION OF EFFECTIVE BARRIER TO PHOTOISOMERIZATION IN ISORHODOPSIN BASED ON VARIOUS KINETIC MODELS OF THE TEMPERATURE AND WAVELENGTH DEPENDENCE OF THE ISORHODOPSIN → BATHORHODOPSIN PHOTOISOMERIZATION QUANTUM YIELD*

Parameter assigned	Model A	Model B	Model C
	Eq. 18	Eq. 19	Eq. 19
E_a (cm^{-1})	70 ± 18	68 ± 13	33 ± 4
E_a (kcal mol^{-1})	0.20 ± 0.05	0.20 ± 0.04	0.10 ± 0.01
Φ_4^{max}	n.a.‡	(0.22)§	0.165 ± 0.003
T_f	n.a.	0.044 ± 0.014	(Eq. 20)
α	n.a.	n.a.	0.008 ± 0.005
β	n.a.	n.a.	4.6 ± 1.1
r^2 (correlation coefficient)	n.a.	0.9206	0.9860
standard deviation	n.a.	0.0097	0.0052

*Error bars listed for model A are standard deviations assigned by using propagation of error associated with the measured values of the quantum yields that appear in Eq. 18. The error bars listed for models B and C are standard deviations assigned from the regression analyses.

‡n.a. indicates not applicable.

§The value of Φ_4^{max} is set equal to the ambient temperature value of Φ_4 (0.22) for model B.

models share the following three assumptions: (*a*) the origin of the wavelength dependence is associated with a finite barrier for photoisomerization in the excited state; (*b*) the quantum yield increases with increasing excitation energy due to the transfer and/or partitioning of a portion of the excess vibrational energy into torsional (C_{9-10}) kinetic energy; (*c*) Boltzmann statistics determines the probability that this energy will be sufficient to surmount the barrier. These assumptions, along with those introduced in deriving Eq. 17, produce the following relationship:

$$\Phi_4(\nu, T) = \Phi_4^{max} \cdot \exp\{-E_a/[kT + T_f(\nu) \cdot (\nu - \nu_0)]\} \quad (19)$$

where $\Phi_4(\nu, T)$ is the quantum yield of I $\rightarrow$ B photoisomerization at excitation ν, Φ_4^{max} is the maximum value of the quantum yield at temperature T, ν_0 is the wavenumber of the system origin (or red edge for severely inhomogeneously broadened absorption bands) and $T_f(\nu)$ is the transfer fraction at excitation energy ν. The latter parameter assigns that fraction of the excess vibronic energy [$= (\nu - \nu_0)$] available to the torsional degree of freedom. The model embodied in Eq., 19 provides for, but does not require, that T_f display an excitation energy dependence.

We will examine two models based on Eq. 19. The two models differ in the extent to which vibronic energy is partitioned into "available energy" (torsional kinetic energy), as well as the choice of Φ_4^{max}. Both models assume that ν_0 equals 17,240 cm^{-1} (λ = 580 nm). This value is clearly to the red of the system origin (see Fig. 1), but our calculations are not overly sensitive to assignment of ν_0 provided the energy is underestimated ($\nu_0 \leq$ origin) rather than overestimated. Thus, we chose a value of ν_0 that purposely underestimates the true system origin energy.

Model B is based on many of the approximations that were adopted in the early development of the kinetic theory of unimolecular reactions (Marcus, 1952; Rice, 1961). Indeed, Eq. 19 can be derived from RRKM theory by adding the radiation bath as an additional source of energy and by assuming that T_f corresponds to the ratio of the effective to total densities of levels (normally defined in terms of vibrational partition functions). We ignore, for the purposes of the present discussion, the fact that T_f will have a temperature dependence, and in the case of model B, we assume T_f is also wavelength independent. Since our primary goal is to determine a realistic value for E_a, we will not attempt to formulate an equation for T_f here. In the absence of a realistic model of the vibrational manifold of the chromophore including anharmonicities for the torsional degrees of freedom, *a priori* assignment of T_f is not realistic. The present study treats T_f as a disposable regression parameter with physical relevance only in qualitative and relative terms. Φ_4^{max} has a more clear-cut definition as the maximum quantum yield for the isorhodopsin $\rightarrow$ bathorhodopsin phototransformation. We assign this parameter a value of 0.22 based on the wavelength independent value observed at ambient temperature (Hurley et al., 1977). A least squares regression analysis of the experimental data presented in Table II yields a value of E_a very close to that obtained based on model A (see Table III). The excellent agreement is likely fortuitous given the level of approximations adopted in both models. Nevertheless, this agreement suggests that the temperature and wavelength dependences in Φ_4 have the same photophysical origin, namely a small (effective) barrier for photoisomerization in the excited state.

The regression analysis predicts T_f = 0.04, which suggests that only 4% of the excitation energy is transferred into "effective vibrational degrees of freedom." Given the low energy of C_{9-10} torsional mode (a mode that will effectively transform into a free rotor mode at energies above E_a), this value is somewhat lower than expected based on simple partitioning calculations. It is likely that the assumption of a wavelength independence in T_f is a rather severe approximation. This assumption is relaxed in the following model.

Model C is based on the same assumptions as model B except Φ_4^{max} and T_f are both assigned via regression procedures. The former is treated as a single valued parameter and the latter is assigned by using the following equation,

$$T_f(\nu) = MIN_{\geq 0}\left[1 ; \frac{\alpha(\nu - \nu_0)^\beta}{(\nu - \nu_0)}\right] \quad (20)$$

where α and β are regression parameters, and the function $MIN_{\geq 0}$ (i ; j) returns the smaller of the two arguments provided i > 0 and $j > 0$, and returns zero if $i < 0, j < 0$ or either argument is undefined (the j argument in Eq. 20 is assumed to be "undefined" for $\nu = \nu_0$). Eq. 20 provides, in essence, a highly flexible form for the transfer fraction while constraining the fraction within the prescribed limits ($0 \leq T_f(\nu) \leq 1$). The results of the least squares fit of the data in column 2 of Table II to model C are presented in Tables II and III and graphed in Fig. 2

Model C predicts a very low barrier (~33 cm^{-1}), roughly half that predicted by models A and B (see Table III). Since model C fits the data better than model B (compare Figs. 2 *d* and *c*), it is tempting to conclude that the barrier calculated by model C is more accurate. We conclude, however, that the barrier calculated by model C is more likely to represent the lower limit for E_a. This position is based primarily on an analysis of the predicted wavelength dependence of the transfer fraction (Fig. 2 *b*) based on the regression fit to Eq. 20. The transfer fraction increases from 0.0 (570 nm) to unity ($\lambda > 470$ nm), indicating that excitation energies to the blue of the latter value are 100% efficient at transferring the excess energy of the photon into the torsional mode. This prediction is highly unlikely, and suggests that the accuracy of the fit associated with model C is due, at least in part, to a physically unrealistic assigned flexibility in $T_f(\nu)$.

Analysis of the results of models A, B, and C (Table III) suggests that the effective barrier for 9-cis $\rightarrow$ 9-trans photoisomerization is ~70 cm^{-1} or 0.2 kcal mol^{-1}.

Although this barrier may appear to be unrealistically small, the excellent agreement between the two constrained models (A and B) supports the assignment. It is instructive to compare this barrier with that observed for retinals in solution by Waddell and Chihara (1981). These investigators studied the effect of temperature on yields for photoisomerization of all-trans → 9-cis, 11-cis, and 13-cis retinal in solution. Procedures analogous to our model A were used to predict barriers of 1.6 – 3.2 kcal mol^{-1} for all-trans retinal photoisomerization (the barrier was dependent upon solvent and cis isomer product). It is clear that the opsin binding site lowers dramatically the excited state barrier. The origin of this effect remains a subject of controversy (Becker and Freedman, 1985; Birge et al., 1987; for a recent review see Sandorfy and Vocelle, 1986).

Oscillator Strengths of the Principal Absorption Bands of Rhodopsin, Isorhodopsin, and Bathorhodopsin

Oscillator strength measures the "allowedness" of an electronic transition. This dimensionless parameter is very sensitive to polyene conformation (Honig et al. 1980) and relatively insensitive to solvent environment (Myers and Birge, 1980), and thus can provide additional information on the geometry of the chromophore within the binding site. For example, the observation of a rhodopsin oscillator strength >0.9 indicates that the 11-cis chromophore is 12-s-trans rather than 12-s-cis (Honig et al., 1980; Birge and Hubbard, 1980; Akita et al., 1980). The oscillator strength is also very sensitive to counterion location (Birge et al., 1987). We will demonstrate that the anomalous oscillator strength observed for isorhodopsin provides insight into the opsin counterion environment.

The analysis of the oscillator strengths of the λ_{max} absorption bands of R, I, and B is shown in Fig. 1. The absorption bands were fit from the red edges to 22,500 cm^{-1} to log-normal curves following the procedures described in Methods. The oscillator strengths were then calculated by using Eq. 11 (see top of Fig. 1). Subsequent corrections to these values were applied by using Eq. 10 and integrating under the difference curves ($\epsilon_{obsv} - \epsilon_{calc}$) (bottom of Fig. 1). The results are given in Table I. Analogous procedures were used to measure the oscillator strengths of the retinal isomers based on the spectra shown in Fig. 4. In order to compare the results with those for R, B, and I the spectra measured in EPA (77 K) were used. The polar solvent EPA is predicted to strongly favor the 11-cis, 12-s-trans conformer over the 11-cis, 12-s-cis con-

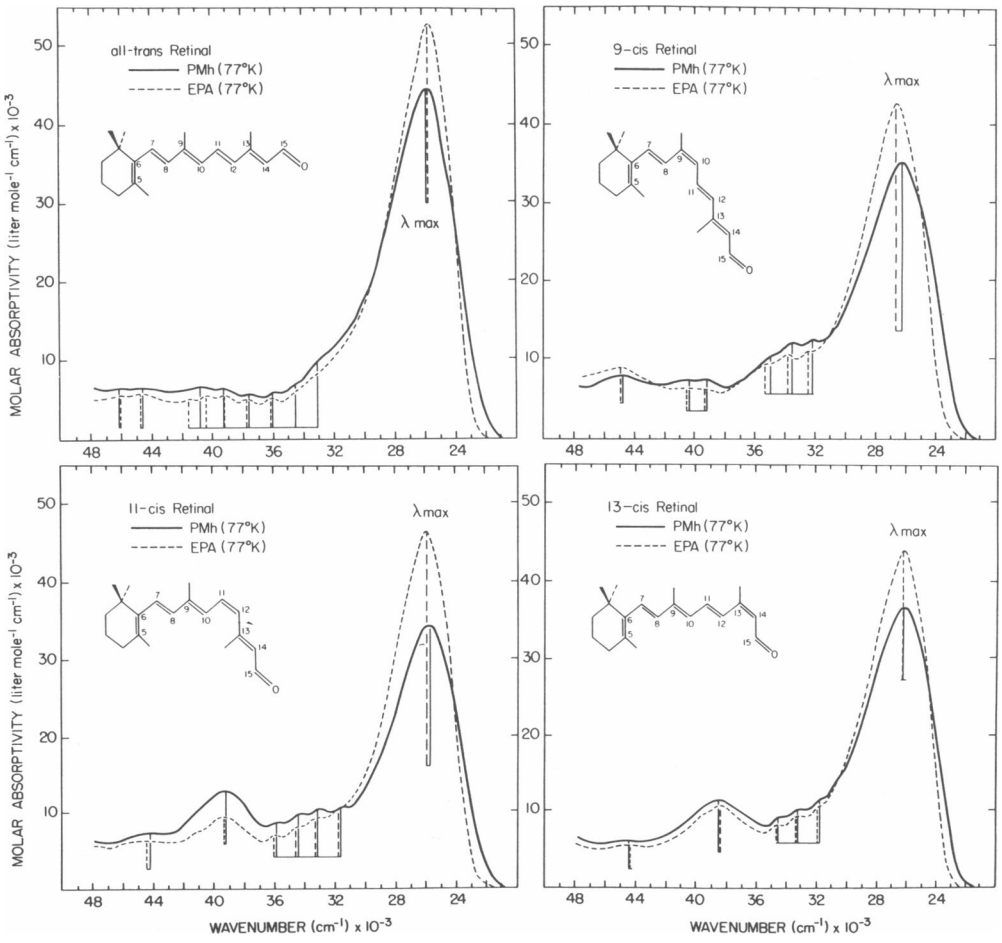

FIGURE 4 Absorption spectra of all-trans, 9-cis, 11-cis, and 13-cis retinal in the mixed polar solvent EPA and the mixed nonpolar solvent PMh at 77 K. Log-normal fits to the EPA spectra are presented in Table IV.

former (Sperling, 1972; Birge, 1981), and this solvent effect is desired since the chromophore in R is known to be 11-cis, 12-s-trans (Callender et al., 1976; Honig et al., 1980; Birge and Hubbard, 1980; Akita et al., 1980). The results of the oscillator strength analysis of the retinals are presented in Table IV. Before analyzing and comparing these results, we will examine the parameters that are predicted based on the log-normal fit.

Interpretation of skewness and bandwidth parameters. The skewness (ρ) is a direct measure of the extent to which the absorption band is asymmetric relative to the absorption maximum:

$$\rho = \frac{(\nu_b - \nu_0)}{(\nu_0 - \nu_r)}, \tag{21}$$

where ν_b is the wavenumber to the blue (higher energy) side of the absorption maximum (ν_0) at which the absorptivity is half that at maximum intensity, and ν_r is defined analogously for the red side. Accordingly, the full-width at half-maximum equals $\nu_b - \nu_r$. A Gaussian intensity distribution is symmetric, which requires $\rho = 1$ (see Methods and Eqs. 12 and 13). Frank-Condon activity of higher energy vibronic transitions will tend to blue shift ν_b relative to ν_0 and thus make $\rho > 1$. However, there does not appear to be any clear relationship between the value of ρ and the geometry and/or extent of vibronic activity for the visual chromophores or the visual pigments. While it is tempting to suggest that the cis-linkages in the chromophores of R and I are responsible for generating a larger ρ than is observed in B, the data of Table IV provide no support for this interpretation. A correlation of ρ with vibronic activity is expected based on model calculations using wavepacket propagation theory. The absence of any relationship in the present case is likely due to the dominance of intramolecular and environmental inhomogeneous broadening in defining the band shape.

The full-width at half-maximum ($\Delta\nu_{FWHM}$) is larger in the visual chromophores (Table IV) than in the pigments (Table I). This difference could arise from a variety of factors including substituent effects (the protein bound chromophores are protonated Schiff bases), conformational effects (the chromophore is locked into a more rigid configuration by the protein matrix than is present in solution), or environmental effects (the solvent environment is more inhomogeneous than the protein environment). It is significant perhaps that $\Delta\nu_{FWHM}$ is larger in both 9-cis retinal and I relative to their all-trans and 11-cis counterparts.

We conclude from an analysis of the isomeric and protein effects on ρ and $\Delta\nu_{FWHM}$ that these two parameters are likely indicative of external (environmental) factors rather than conformational factors. We will return to this issue subsequently.

Interpretation of oscillator strengths. The salient observation is that 9-cis retinal has the smallest oscillator strength of the four retinal isomers (Table IV),

TABLE IV
SPECTROSCOPIC PROPERTIES OF ALL-TRANS, 9-CIS, 11-CIS AND 13-CIS RETINAL IN EPA AT 77K

Measurement	All-trans	9-cis	11-cis	13-cis
λ_{max} (nm)	387	380	389	382
$\epsilon(\lambda_{max})$*	52.6	43.2	45.7	44.2
f(λ_{max} band)‡	1.17	0.98	1.04	1.06
f(λ_{max} band) (lit.)§	1.20	1.00	1.03	1.05
log-normal fit‖				
ν_{max} (cm^{-1})	25,670(±10)	26,320(±14)	25,530(±10)	26,160(±15)
ϵ (ν_{max})	51.8	42.2	44.9	43.2
error in ϵ (ν_{max})	±0.2	±0.2	±0.2	±0.2
$\Delta\nu_{FWHM}$ (cm^{-1})	4,670(±30)	4,840(±70)	4,767(±30)	5,060(±70)
ρ (skewness)	1.69	1.62	1.69	1.74
Error in ρ (skewness)	±0.02	±0.03	±0.02	±0.04
r^2	0.9996	0.9992	0.9996	0.9992
f (log-normal)	1.1692	0.9769	1.0393	1.0604
$\Delta f[\Sigma(\epsilon_{obsv}-\epsilon_{log\text{-}normal})]$¶	−0.0011	−0.0009	−0.0010	0.0010

*Molar absorptivities, ϵ, are listed in $M^{-1}\,cm^{-1} \times 10^{-3}$. Errors are estimated to be 5% plus 0.1.

‡Oscillator strength obtained by using log-normal fit (Eq. 11) and subsequently applying correction integral as described in text. The fit was carried out from 350–500 nm, and the calculated and correction terms are listed in the last two rows of the appropriate column.

§Calculated from the data measured for spectra (EPA, 77 K) presented in Tables I and II of Sperling (1972).

‖Parameters listed were obtained from log-normal fit of absorption spectra from 350–500 nm and may not agree precisely with the results of the direct analysis of the absorption spectra.

¶Correction to the log-normal oscillator strength [f(log-normal)] obtained by numerically integrating under the difference curve $\epsilon_{obsv}-\epsilon_{log\text{-}normal}$ from 350 to 500 nm (see text).

but that isorhodopsin (which contains the 9-cis protonated Schiff base chromophore) has the largest oscillator strength of the three pigments. The former is anticipated based on conformational arguments (Honig et al., 1980). The observation that isorhodopsin has the largest oscillator strength of the three pigments is anomalous.

The excellent agreement of our data for the retinals with those of Sperling (1972) supports our assignment for the chromophores. However, our oscillator strength measurements on the pigments are the critical issue here, and further literature confirmation of our results is desirable. All literature spectra of R and I that we are aware of are charactrerized by two features (*a*) the absorption maximum of I is blue shifted and exhibits a higher molar absorptivity relative to the absorption maximum of R, and (*b*) the FWHM (cm^{-1}) of the I specturm is slightly larger than that observed for R (Wald and Brown, 1953; Yoshizawa and Wald, 1963; Yoshizawa, 1972; Crouch, et al., 1975; Mao et al., 1980). The literature data yield f(I) ~ 1.1 f(R). Our value of f(I) = 1.13 f(R) (see Table I) is in good agreement. Finding consistency in the literature concerning the absorption spectrum of B is not possible. The original studies of Yoshizawa and Wald (1963) indicate f(I) ≥ f(B) > f(R) whereas the more recent studies of Mao et al. (1980) indicate f(B) ≥ f(I) > f(R). A lack of agreement on this issue is not surprising given the difficulty in calculating the spectrum of B (it is not possible to generate photostationary state mixtures containing more than ~65% B, and uncertainty in the amount of B is a further source of error). Fortunately, the conclusions of this study are not affected by ambiguity in the relative oscillator strengths of B or I, provided f(I) ~ f(B) ~ 1.1f(R).

It would be preferable to compare oscillator strengths measured for protonated Schiff base isomers in solution with the pigment values. Unfortunately, the preparation of isomerically pure PSB isomers is extremely difficult. In particular, the 9-cis and 11-cis protonated Schiff bases are highly thermal- and photo-labile, and preparation of verifiably pure samples in solution has eluded our best efforts. We believe that using the retinal isomers as model compounds is adequate for calibrating our theoretical methods (see below).

Theoretical Analysis of the Specrtroscopic and Photochemical Properties of Rhodopsin, Bathorhodopsin, and Isorhodopsin

INDO-PSDCI molecular orbital theory has been very successful in rationalizing the spectroscopic and photochemical properties of the visual chromophores, both in solution and in the opsin binding site (Birge and Hubbard, 1980, 1981; Birge 1981; Birge et al. 1982, 1987). If we assume a 12-s-trans conformation for the 11-cis chromophore, INDO-PSDCI procedures reproduce the correct oscillator strength ordering observed for the retinal isomers in EPA(77k) (Table V).

We also used INDO-PSDCI molecular orbital theory to calculate oscillator strengths of the λ_{max} bands for chromophores in various model binding sites. The details of this study are presented below, and the results for the most successful model (Fig. 5) are presented in Table V. The calculations predicted correctly the increase in the oscillator strength of I relative to R because our model was adjusted until this experimental observable was repro-

TABLE V
COMPARISON OF OBSERVED AND CALCULATED OSCILLATOR STRENGTHS FOR SELECTED COMPOUNDS

Compound	Observed*	INDO-PSDCI‡	Assumed geometry§
All-trans retinal	1.17	1.22	6-s-cis (58°)
9-cis retinal	0.98	0.98	6-s-cis (58°)
11-cis retinal	1.04	0.99¶	6-s-cis (41°),12-s-trans (39°)
13-cis retinal	1.07	1.11	6-s-cis (58°)
All-trans retinyl PSB‖	0.90	0.95	6-s-cis (58°)
Rhodopsin	0.98	0.86	Fig. 5 *a*.
Bathorhodopsin	1.07	0.91–1.26**	Fig. 5 *b*.
Isorhodopsin	1.11	1.15	Fig. 5 *c*.

*Data are taken from Table I (pigments) or Table IV (retinal isomers) unless indicated otherwise.

‡Calculations include all single excitations below 15 eV and all double excitations below 20 eV. All other details as in Birge and Hubbard (1980, 1981).

§Assumed geometry indicates major torisonal assignments and their out-of-plane dihedral angles (reduced to the first quadrant for convenience). All other out-of-plane distortions are <5°, and are assigned by using the crystal geometry of all-trans retinal (Hamanaka et al., 1972) to assign all-trans, 9-cis, and 13-cis geometries (with the exception of the salient cis double bond) and the crystal geometry of 11-cis retinal (Gilardi et al., 1972) to assign 11-cis, 12-s-trans retinal (with the appropriate 12-s-cis to 12-s-trans modification).

‖Observed and calculated results from Fig. 6 of Birge et al. (1987). The calculated oscillator strength is very sensitive to counterion location.

¶The oscillator strength calculated for 11-cis, 12-s-trans retinal is sensitive to the 12-s-trans dihedral angle and increases to 1.07 for a planar 12-s-trans geometry.

**The oscillator strength calculated for bathorhodopsin is sensitive to the extent to which energy storage is partitioned into conformational distortion of the chromophore versus charge separation (see text). The range given defines the approximate limits: 0.91 (majority of energy is stored in conformational distortion), 1.26 (majority of energy is stored in charge separation).

duced. The oscillator strength calculations on B are very sensitive to the extent to which charge separation energy is allowed to partition into conformational distortion (see Table V). As noted below, this sensitivity was exploited in developing our model for energy storage in the primary photoproduct.

The origin of the barrier in the isorhodopsin → bathorhodopsin excited state surface. Analysis of the ground and excited state torsional potentials associated with the primary photochemistry of R and I is presented in Table VI. The first two rows of Table VI present ground and first excited singlet state barriers for an isolated protonated Schiff base (no counterion, vacuum conditions). It is surprising to note that while both 9-cis and 11-cis species have negative barriers for cis → trans photoisomerization, the 9-cis isomer has a more negative barrier (row 2, Table VI). This result is unexpected given the observation that I, but not R, exhibits a barrier to photoisomerization. The origin of the barrier in I is predicted to arise from electrostatisc effects associated with the interaction of the counterion and the protonated species.

One of the primary driving forces responsible for the rapid and efficient photochemistry of rhodopsin is associated with strong electrostatic interactions between the chromophore and a fixed counterion (Birge and Hubbard, 1980). While it is not known which specific amino acid provides the counterion, only three canonically anionic residues are predicted to be located in proximity to the retinyl chromophore (Asp 83, Glu 122, and Glu 134; Hargrave et al., 1984). Fortunately, all three of these residues would provide very similar electrostatic interactions, and our simplified model of the counterion using a CH_3—CO_2^- residue (Fig. 5) is equally appropriate to aspartic or glutamic acid residues. The larger cis → trans excited state barrier in isorhodopsin can be explained without precise assignment of the counterion location by noting that the C_{15}=NH_2 terminus portion of the 9-cis chromophore experiences a much smaller charge polarization during isomerization in the lowest singlet state than is predicted for the 11-cis chromophore of rhodopsin (Table VI). An important component to the driving force promoting photoisomerization is the fact that upon excitation, the polyene moiety near the C_{15}=NH_2 terminus region experiences an influx of negative charge upon vertical excitation (row 3 and 4, Table VI), and that upon torsional distortion about the appropriate cis linkage, a large shift of negative charge out of this region is predicted (row 5, Table VI). This charge reorganization helps drive the photoisomerization by preferential stabilization of the 9- or 11-orthogonal conformations (note that the negatively charged counterion is fixed and thus repulses the planar S_1 conformation, but stabilizes the orthogonal S_1 conformation). The analysis presented in Table VI suggests that the electrostatic driving force for photoisomerization is ~1.5 times larger in rhodopsin than in isorhodopsin. This electrostatic effect is predicted to have a 1.2 kcal mol^{-1} differential effect on the S_1 potential surface (row 7, Table VI). In the absence of a detailed model of the rhodopsin binding site, a more accurate theoretical analysis is not possible. An energy difference of 1.2 kcal mol^{-1} would be sufficient to produce a 0.2 kcal mol^{-1} activation barrier along the 9-cis → 9-trans S_1 surface if the shape of the rhodopsin excited state surface predicted by Birge and Hubbard (1980, 1981) is reasonably accurate.

Interpretation of energy storage is isorhodopsin and bathorhodopsin. Recent photocalorimetric studies have investigated energy storage in B formed from R, as well as in B formed from I (Schick et al., 1987). These studies are consistent with previous investigations by Cooper (1979a, b), and the salient results are shown in Fig. 3. Although no direct measurements of the conformational energies of the isolated chromophores have been reported, indirect experimental measurements and theoretical calcu-

TABLE VI
ANALYSIS OF GROUND AND EXCITED STATE TORSIONAL POTENTIALS ASSOCIATED WITH RHODOPSIN AND ISORHODOPSIN PRIMARY PHOTOCHEMISTRY BASED ON INDO-PSDCI MOLECULAR ORBITAL THEORY

Calculated Property*‡	11-cis → 11-trans	9-cis → 9-trans
S_0[E(⊥) − E(∥)] (no CTN) (kcal mol^{-1})	29	38
S_1[E(⊥) − E(∥)] (no CTN) (kcal mol^{-1})	−4.6	−5.8
Σ[q(9,11) . . . q(N)] (S_0) (∥)	223	269
Σ[q(9,11) . . . q(N)] (S_1) (∥)	−188	−115
Σ[q(9,11) . . . q(N)] (S_1) (⊥)	669	426
S_1[E(⊥) − E(∥)] (CTN) (kcal mol^{-1})	−10.2	−9.1
S_1[E(⊥) − E(∥)] (CTN + CD) (kcal mol^{-1})	−6.1	−4.9

*The following symbols are used to describe the calculations and geometries: E(⊥) = total system energy for $\Phi(C_9 = C_{10})$ or $\Phi(C_{11} = C_{12})$ orthogonal geometry, E(∥) = total system energy for $\Phi(C_9 = C_{10})$ or $\Phi(C_{11} = C_{12})$ cis planar geometry, (no CTN) = calculation does not include counterion, Σ[q(9,11) . . . q(N)] = sum of atomic charges on the carbon and nitrogen atoms (electron units × 10^3) in the segment that rotates away from the counterion during formation of bathorhodopsin (for 11-cis, segment is C_{13} . . . N; for 9-cis, segment is C_{11} . . . N; see Fig. 5), (CTN) = calculation includes the counterion shown in Fig. 5, (CTN + CD) = calculation includes the counterion and conformational distortion energy.
‡Calculations include all single excitations below 15 eV and all double excitations below 20 eV. All other details as in Birge and Hubbard (1980, 1981).

lations indicate that 9-cis and 11-cis retinal have similar enthalpies that are ~1 kcal mol^{-1} above that of all-trans retinal (for reviews see Birge, 1981; Ottolenghi, 1980). Despite the uncertainties, it is clear that the vast majority of the energy differences observed for the pigments (Fig. 3) are associated with protein-chromophore interactions. A number of studies have addressed the issue of opsin recognition, binding site geometry and energy storage (Baasov and Sheves, 1985; Bagley et al., 1985; Barry and Mathies, 1987; Birge, 1981; Birge and Hubbard, 1981; Cooper, 1979a, b; Deng and Callender, 1987; Eyring et al., 1982; Honig et al., 1979a, b; Liu et al., 1984; Matsumoto and Yoshizawa, 1978; Ottolenghi, 1980; Palings et al., 1987; Sandorfy and Vocelle, 1986; Schick et al., 1987; Smith et al., 1987 and Warshel and Barboy, 1982). There is no universally accepted model of energy storage, and some models emphasize energy storage due to charge separation (e.g., Honig et al., 1979a, b) while others emphasize energy storage due to conformational distortion (e.g., Birge and Hubbard, 1980, 81). Virtually all models recognize that both mechanisms contribute, and discussions center on the extent to which one mechanism dominates the other. The present investigation has the potential of partially resolving the issue, provided one accepts the premise that the opsin binding sites of R, B, and I are identical (see above for discussion concerning the viability of that assumption). This potential derives from the fact that the observed absorption maxima (Table I), oscillator strengths (Table I) and enthalpies (Fig. 3; Cooper, 1979a, b; Schick et al., 1987) are mechanistically interrelated such that the origins of energy storage can be deduced.

Models of the Opsin Binding Site. We used INDO-SCF-MO (Pople et al., 1967) and INDO-PSDCI (Birge and Hubbard, 1980, 81) procedures to test various models of the binding site and predict theoretically the molecular origins of the spectroscopic and thermodynamic properties of R, B, and I. A variety of binding site proposals were investigated including those of Bagley et al. (1985), Barry and Mathies (1987), Birge and Hubbard (1980, 81), Birge et al. (1987), Honig et al. (1979a), Kakitani et al. (1985), LeClercq and Sandorfy (1981), Liu et al. (1984), Liu and Asato (1985), Palings et al. (1987), Rothschild et al. (1983), Sheves et al. (1986) and Warshel and Barboy (1982). Calculations were carried out by assuming that the b-ionylidene ring, the α and β carbon atoms of the lysine residue, and all of the atoms of the counterion, were fixed spatially. The counterion, a glutamic or aspartic acid residue (Hargrave et al., 1984), was approximated by using a CH_3—CO_2^- moiety. The binding site model shown in Fig. 5 provides the best agreement with experiment.

Although the model shown in Fig. 5 does not account quantitatively for all of the experimental observables (see below), none of the literature models tested was more successful. In the absence of knowledge of the tertiary structure of the protein as well as a computer capable of handling a SCF molecular orbital simulation of the complete binding site, we must be satisfied with more qualitative models. The model shown in Fig. 5 is capable of rationalizing all of the above observations. The key features and predictions of this model are summarized below:

(*a*) The counterion (abbreviated as CTN) is not intimately associated with the imine proton in R (Fig. 5 *a*), B (Fig 5 *b*), or I (Fig. 5 *c*). The counterion lies underneath the plane of the chromophore, and the primary chromophore-counterion electrostatic interactions involve C_{15}—CTN and C_{13}—CTN (see Fig. 5 *c*). These specific interactions between the chromophore and the counterion in isorhodopsin are responsible for the anomalous oscillator strength of I relative to R and B. It is difficult to quantify the extent to which the counterion location affects the blue shift of the isorhodopsin absorption maximum. A major portion of the blue shift may be intrinsic to the 9-cis conformation. Note that the absorption maximum of 9-cis retinal lies almost 800 cm^{-1} to the blue of the absorption maximum of 11-cis retinal (Table IV). For comparison, the absorption maximum of I lies ~525 cm^{-1} to the blue of the absorption maximum of R. Interaction of the counterion with the chromophores in R and I may be of secondary importance in determining the blue shift of the isorhodopsin maximum. Indeed, counterion interactions may decrease the extent of the blue shift, an observation that is consistent with the prediction that the chromophore in R is more electrostatically stabilized by the counterion than is the chromophore in I (see below).

(*b*) The presence of a small activation barrier (~0.2 kcal mol^{-1}) in the 9-cis → 9-trans excited state surface is associated with the location of the counterion as well as the intrinsic photophysical properties of the 9-cis chromophore. The principal difference between the 11-cis → 11-trans photoreaction surface and the 9-cis → 9-trans photoreaction surface is the lack of effective electrostatic stabilization of distorted 9 = 10 conformations due to incomplete charge polarization in the orthogonal species.

(*c*) Hydrogen bonding to the imine proton, if present, does not involve the counterion. A number of studies have indicated that the imine proton is hydrogen bonded (Bagley et al. (1985), Barry and Mathies (1987), Rothschild et al., (1983), Sheves et al. (1986)) in all three pigments. We conclude that water in the active site, or secondary interactions with the protein (not involving the CTN), are responsible. The presence of water in the binding sites of rhodopsin as well as bacteriorhodopsin has been proposed previously by others (Hildebrandt and Stockburger [1984], Rafferty and Shichi [1981], Warshel and Barboy [1982]).

(*d*) All photochemical transformations involve one-bond photoisomerizations. This prediction is based on the observation of a very small excited state barrier for the I → B photoreaction (see above), a negative barrier for the R → B phototransformation, coupled with the theoretical prediction that all two-bond processes have significant S_1

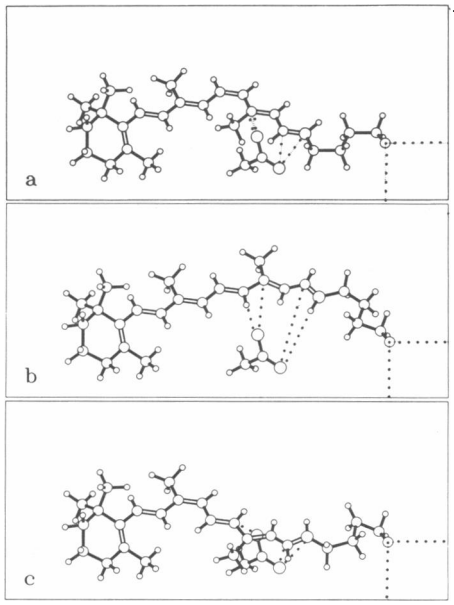

FIGURE 5 Molecular models of the chromophore, lysine, and counterion geometries in (*a*) rhodopsin (R), (*b*) bathorhodopsin (B), and (*c*) isorhodopsin (I) based on the experimental and theoretical (INDO-PSDCI) results of this study. The entire β-ionylidene ring, the α-carbon of the lysine residue and the counterion are assumed to be held stationary by the protein matrix during the phototransformations, so that all geometric relaxation is localized within the $C_7..N_{16}..\beta—C_{lys}$ fragment. Note that the counterion (an aspartic or glutamic acid residue) is approximated in these calculations by using a $CH_3—CO_2^-$ moiety. The counterion (CTN) is not intimately associated with the imine proton in R, B, or I. The counterion lies underneath the plane of the chromophore in R and I, and the primary chromophore-counterion electrostatic interactions involve C_{15}—CTN and C_{13}—CTN. These interactions are directly responsible for the blue shifted absorption maximum and the anomalous oscillator strength of I relative to R and B. Rhodopsin in energetically stabilized relative to isorhodopsin due to both electrostatic interactions (~2 kcal mol^{-1}) and conformational distortion (~3 kcal mol^{-1}) to give $\Delta H_{I\text{-}R}$ = ~5 kcal mol^{-1}. Energy storage in bathorhodopsin ($\Delta H_{B\text{-}R}$ = ~32 kcal mol^{-1}) is ~60% conformational distortion and 40% charge separation.

barriers while one-bond processes have small to negative S_1 barriers (Birge and Hubbard, 1980, 1981 and to be published).

(*e*) Rhodopsin is energetically stabilized relative to isorhodopsin due to both electrostatic interactions and conformational distortion, both favoring stabilization of R. The INDO-PSDCI calculations suggest that rhodopsin chromophore-CTN electrostatic interactions provide an enhanced stabilization of ~2 kcal mol^{-1} relative to I. Conformational distortion of the 9-cis chromophore-lysine system accounts for ~3 kcal mol^{-1}.

(*f*) Energy storage in bathorhodopsin is ~60% conformational distortion and 40% charge separation. These percentages are based on an energy minimization of the chromophore-lysine residue of Fig. 5 *b* using 35 internal degrees of freedom while monitoring absorption maximum, oscillator strength, and electrostatic energy storage. These three variables were compared with experiment by using R as a standard so that the INDO-PSDCI procedures were optimizing differences rather than absolute values. Best agreement with experiment was obtained for all three variables when energy storage was partitioned as follows: charge separation (~12 kcal mol$^-$), intrachromophore-lysine conformational distortion (~10 kcal mol^{-1}), and chromophore-protein conformational distortion (~10 kcal mol^{-1}). It should be noted that our model does not define the source of the latter intramolecular repulsion energy since the chromophore-protein interactions cannot be specified in the absence of a more complete binding site model. We arrive at the latter value by reference to the observed energy storage measurements (Cooper, 1979a, b; Schick et al., 1987). Our model predicts that the majority of the chromophore-protein conformational distortion energy involves interaction of the $C_{13}(—CH_3)=C_{14}—C_{15}=N$-lysine moiety with nearby (unknown) protein residues. (The possibility that the methyl group attached to C_{13} is a primary contributor is being studied currently by using pulsed laser photocalorimetry.)

(*g*) Strong interactions between the counterion and the chromophore in R and I will generate weak, but potentially observable, charge-transfer bands in the near infrared (see Fig. 6). Although our binding site model differs significantly from that proposed by LeClercq and Sandorfy (1981), we agree with their basic prediction that low-lying charge transfer states are likely to be present in rhodopsin. A comparison of semi-empirical and *ab-initio* molecular orbital calculations, however, indicates that the INDO-PSDCI calculations may overestimate the oscillator strengths by factors of two (or more) due to basis set inflexibility (the valence basis set does not define accurately the radial electron distribution on the R-CO_2-oxygen atoms). The INDO-PSDCI calculations appear to be more accurate in predicting transition energies. The key predictions are the presence of a weak, but potentially observable charge-transfer transition at 859 nm (11,640 cm^{-1}) in I (see Fig. 6) and an analogous, but slightly weaker band at 897 nm (11,150 cm^{-1}) in R. Both transitions involve the transfer of an electron from the counterion into low-lying π^* molecular orbitals. Spectroscopic assignments of one or more charge transfer transitions in R or I would be potentially useful in determining the location of the counterion(s) in the opsin binding site. Further experimental and theoretical work in this area is therefore important.

Many of the above predictions are new while others differ in significant areas with previous literature models. Although a global discussion is not possible, the following section is devoted to a brief analysis of related literature studies with the goal of identifying and resolving some of the salient issues.

Comparison of Our Binding Site Model with Literature Models

A majority of literature models of the opsin binding site, including our earlier models (Birge and Hubbard, 1980,

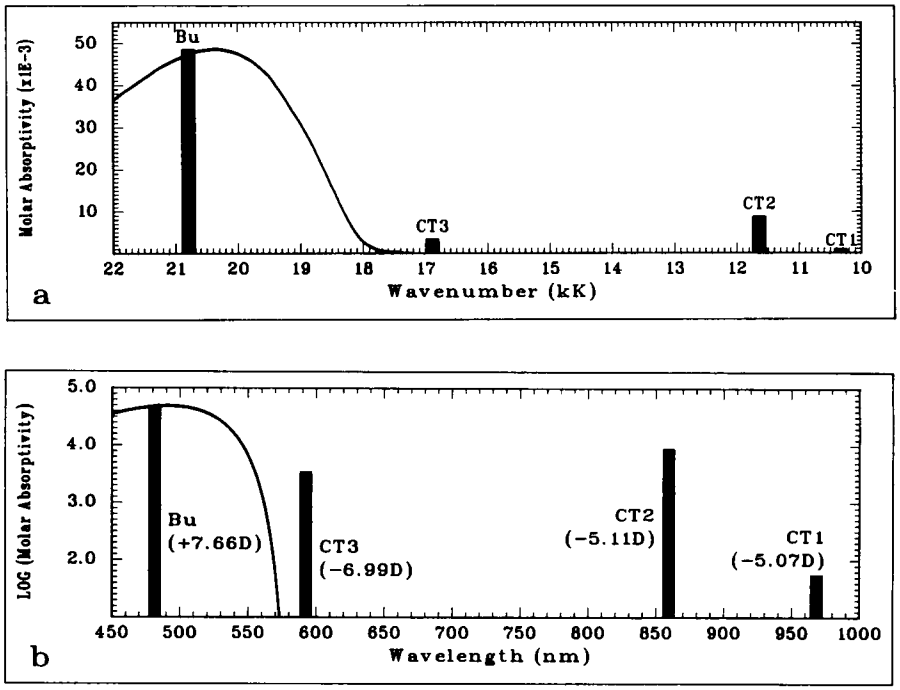

FIGURE 6 INDO-PSDCI theory predicts that three charge transfer transitions occur in isorhodopsin (Fig. 5 *c*) at energies below the lowest-lying $\pi^* \leftarrow \pi$ transition ("$^1B_u^{*+}$" $\leftarrow S_o$). These transitions are labelled CT1, CT2, and CT3 and their calculated location in wavenumbers (*a*) and wavelength (*b*) are indicated by using rectangles the heights of which represent the linear absorptivity (*a*) or log (absorptivity) (*b*) relative to the calculated value of the "$^1B_u^{*+}$" $\leftarrow S_o$ transition (labelled B_u). The absorption spectrum of isorhodopsin (Fig. 1) in the 17–22 kK region is shown for comparison. The calculated change in dipole moment upon excitation is given in parentheses (Debyes) in *b*. These calculations were carried out by assuming a vacuum environment. The protein binding site is predicted to red shift those transitions that generate an increase in dipole moment upon excitation. Comparison of INDO–PSDCI and extended basis set *ab-initio* molecular orbital calculations predicts that the former theoretical procedures (used here) will overestimate the allowedness of charge transfer transitions.

1981), assume that the external counterion is hydrogen bonded to the imine proton in rhodopsin. The results of the present study suggest that the counterion is beneath the plane of the chromophore (see Fig. 5). The Raman and Fourier-transform infra-red (FTIR) studies of the C_{15}=NH stretching modes in R, B and I should yield information about the extent to which the imine proton is interacting with the counterion (Baasov et al., 1985, 1987; Bagley et al., 1985; Barry and Mathies, 1987; Deng and Callender, 1987; Kakitani et al., 1983, 1985; Rothschild et al., 1983; and Smith et al., 1985, 1987b). Excellent discussions of recent work in this field can be found in Palings et al. (1987), Deng and Callender (1987), Bagley et al. (1985), and Rothschild et al. (1983). Selected vibrational assignments for R, B, and I as well as the corresponding protonated Schiff bases in solution are presented in Table

TABLE VII
SELECTED LITERATURE VIBRATIONAL ASSIGNMENTS AND OBSERVED FREQUENCIES (CM^{-1}) FOR THE ALL-TRANS, 9-CIS AND 11-CIS PROTONATED SCHIFF BASES AND FOR THE CORRESPONDING VERTEBRATE OPSIN PIGMENTS*

	11-cis		all-trans		9-cis	
Mode‡	PSB	R	PSB	B	PSB	I
C_{15} – NH str	1,658(w)	1,657(w)	1,657(w)	1,655(w)	1,659(w)	1,655(w)
C_{15} – ND str		1,624(w)	1,632(w)	1,625(w)		1,631(w)
ND Shift		33	26	31		24
$C_8 - C_9$ str	1,271(s)	1,217(s)	1,194(s)	1,214(s)	1,204(s)	1,206(s)
$C_{10} - C_{11}$ str	1,093(w)	1,098(w)	1,159(m)	1,166(w)	1,137(m)	1,154(s)
$C_{12} - C_{13}$ str	1,237(s)	1,239(s)	1,237(w)	1,240(m)	1,238(m)	1,242(s)
$C_{14} - C_{15}$ str	1,190(w)	1,190(w)	1,191(w)	1,210(w)	1,189(s)	1,206(s)
$(C = C)_{sym}$ str	1,556(s)	1,547(s)	1,563(s)	1,536(s)	1,567(s)	1,549(s)
$C_{13} = C_{14}$ str		1,581(m)		1,578(w)		1,585(w)
$C_9 = C_{10}$ str		1,599(m)	1,596(w)	1,595(w)		1,599(m)
$C_7 = C_8$ str		1,608(w)				
$C_5 = C_6$ str		1,636(w)	1,612(w)	1,629(w)		1,636(w)

*Data are compiled from Bagley et al. (1985), Deng and Callender (1988), and Palings et al. (1987). When literature assignments differed, averages of the literature values are reported. Relative Raman line intensities are listed in parentheses s, strong; m, medium; w, weak.

‡Modes are defined based on the principal $C - C$, $C = C$ or $C = N$ stretching (str) normal mode eigenvectors. In most cases, other stretching and bending modes contribute to the vibrational band in significant proportion (see Eqs. 22–26, Smith et al., 1985 and Deng and Callender, 1988). Accordingly, these assignments are very approximate and are used primarily for labelling convenience (see text). The abbreviation $(C = C)_{sym}$ Str refers to the strongly Raman active mode, or collection of overlapping modes, involving primarily in phase (symmetric) stretching motions of $C_7 = C_8$, $C_9 = C_{10}$, and $C_{11} = C_{12}$ bonds.

VII. It is remarkable that the C_{15}=NH modes in R, B, and I are so close in frequency (top row, Table VII). Deuterium substitution shifts this mode in I relative to R and B, but the fact that the C_{15}=ND modes in R and B are nearly identical is surprising. If this stretching mode is sensitive to hydrogen bonding to the imine proton (as is generally believed regardless of force field assignments, Lopez-Garriga, 1986; Smith et al., 1987; Deng and Callender, 1987), it is difficult to rationalize identical C_{15}=ND modes in R and B with simultaneous interaction of the counterion with the imine proton in R and charge separation and therefore decreased interaction in B. Our model avoids this inconsistency by proposing that the counterion is beneath the plane of the chromophore, and thus the environment of the imine proton is not affected significantly upon photoisomerization (see Fig. 5). Hydrogen bonding with the imine proton, if it exists, could be associated with water in the binding site or interaction of the chromophore with secondary residues within the binding site. We explore this issue in detail in the following section.

Hydrogen bonding to the imine proton. It is generally proposed that a large ν_{C-N} deuterium (ND shift) isotope shift is characteristic of strong hydrogen bonding to the imine proton (Palings et al., 1987; Deng and Callender, 1987; Bagley et al., 1985). Based on this argument, hydrogen bonding is strongest in R (ND shift ~33 cm^{-1}), strong in B (ND shift ~30 cm^{-1}) and moderately strong in I (ND shift ~24 cm^{-1}). As comparison, the all-trans protonated Schiff base (ATRPSB) in methanol exhibits a ND shift of ~26 cm^{-1} (Table VII). Spectroscopic studies of ATRPSB indicate that the counterion is intimately associated with the imine proton in nonpolar environments (Birge et al., 1987). The work of Blatz (1972) suggests that in highly polar, strongly hydrogen-bonding solvents, the counterion is highly solvated and the imine proton is hydrogen bonded with the solvent. The ND shift has been measured for ATRPSB in both environments and differs by only 3 cm^{-1} (Smith et al., 1985; Palings et al., 1987; Deng and Callender, 1987). One concludes that the ND shift while diagnostic of hydrogen bonding, is not sensitive to the *nature* of the hydrogen bond. Furthermore, a quantitative relationship between the ND shift and the strength of a hydrogen bond to the imine proton has not been firmly established (see Kakitani et al., 1983; Lopez-Garriga et al., 1986; Deng and Callender, 1987).

Although the ND shift is largest in R, it drops by only 2 cm^{-1} in going from R to B. This difference is anomalously small for an isomerization moving the —C_{15}=NH— moiety away from a fixed counterion. Any attempt to maintain a strong hydrogen bond between the imine proton and the counterion following a one-bond 11-cis → 11-tans photoisomerication will fail to accommodate the observed oscillator strengths and bathochromic shifts.

Many proponents of hydrogen bonding between the counterion and the imine proton in R suggest that the imine proton is hydrogen bonded to an uncharged protein residue in B. This model accommodates the bathochromic shift, but does not explain adequately the remarkable similarity of ν_{C-NH} and ν_{C-ND} in R, B, and I (Table VII). One concludes, based on the force field calculations of Deng and Callender (1987), and the model compound studies of Baasov et al. (1985, 1987), that ν_{C-NH} and ν_{C-ND} are rather sensitive to the charge on the hydrogen bonding species. The above model is also incapable of rationalizing a weaker hydrogen bond to the counterion along with a blue shifted absorption maximum in I. We suggest that a detailed evaluation of the ν_{C-N} and ND shift data (rows 1–3, Table VII) does not support hydrogen bonding of the imine proton to the counterion. We suggest that water in the active site, or secondary interactions with the protein (not involving the counterion) are responsible for the observed ND shifts (Table VII).

Counterion interactions and energy storage. The Raman (Palings et al., 1987) and FTIR (Bagley et al., 1985) data support the s-trans, C=N anti structures adopted in Fig. 5 for R, B, and I. What remains unresolved is the extent to which the vibrational assignments can support (or contradict) our assignment of counterion location and our analysis of energy storage. The fingerprint vibrations are nominally assigned to single bond stretching modes (e.g., Table VII), but extensive delocalization of the mode structure makes the vibrations sensitive to structure. For example, the calculations of Smith et al. (1985) yield the following assignments for the all-trans protonated Schiff base fingerprint region:

$$\begin{aligned} Q_A(C_8—C_9) = {} & 0.15(8–9) - 0.74(10H) + 0.08(10–11) \\ & + 0.07(14–15) - 0.07(9—CH_3) \\ & - 0.05(11 = 12) - 0.04(9 = 10) \end{aligned} \quad (22)$$

$$\begin{aligned} Q_A(C_{10}—C_{11}) = {} & 0.27(10–11) + 0.32(11H) \\ & - 0.12(8–9) - 0.03(14–15) \end{aligned} \quad (23)$$

$$\begin{aligned} Q_A(C_{12}—C_{13}) = {} & 0.12(12–13) - 0.83(14H) \\ & - 0.34(12H) + 0.08(14–15) \\ & - 0.04(13—CH_3) \\ & - 0.04(13=14) + 0.03(11=12) \end{aligned} \quad (24)$$

$$\begin{aligned} Q_A(C_{14}—C_{15}) = {} & 0.26(14–15) - 0.35(15H) \\ & - 0.32(12H) - 0.27(11H) - 0.11(12–13) \end{aligned} \quad (25)$$

where $(m - n)$ represents a single bond stretch coordinate for atoms m and n, $(m = n)$ is similarly defined for a double bond stretch coordinate, H represents a hydrogen in-plane rock, and $(m—CH_3)$ is a methyl stretching coordinate. A cursory examination of Eqs. 22–25 indicates clearly that these vibrations are sensitive to a large number of force constants. From a different perspective, it is far from

obvious that fingerprint vibrations will be overly sensitive to external charge location given the extensive delocalization and dependence on σ-dominated (single bond) rather than π-dominated (double bond) force constraints. INDO-PSDCI calculations indicate that gross changes in counterion locations (e.g., Figs. 5 *b* vs. 5 *c* of Birge, et al., 1987) have modest effects on σ-dominated force constants unless covalent or hydrogen bonding interactions are established. The counterion interactions of Fig. 5 are all soft in the sense that they have a global delocalization but no strong influence on the σ electron distribution. We therefore disagree with the statement of Palings et al. (1987) that the mode invariance of the C_{14}—C_{15} fingerprint band in 11-cis PSB and in rhodopsin does not support the presence of a negative charge near C_{13} in rhodopsin. We do support the observation that the fingerprint assignments indicate that the opsin bound chromophore in R is not distorted and has a structure very similar to that found for the solution based 11-cis PSB in polar solvent

Our calculations predict that the ethylenic stretches will be much more sensitive to counterion location, because these modes are sensitive to changes in π-dominated force constants. It has long been recognized that the Raman intense $(C{=}C)_{sym}$ stretch changes linearly with absorption maximum of visual and bacterial pigments (see Baasov and Sheves, 1985, for a recent discussion). Force field studies indicate that the $(C{=}C)_{sym}$ stretch is a delocalized mode with major contributions from $C_7{=}C_8$, $C_9{=}C_{10}$, and $C_{11}{=}C_{12}$ sketches (Smith, et al. 1985; Deng and Callender, 1987). A series of less Raman active asymmetric C=C stretches extend to higher frequencies and are slightly more localized (Table VII). These modes are usually too weak to observe in the chromophores in solution, but the protein matrix enhances these modes, particularly in rhodopsin and isorhodopsin (Table VII). The 1,599 cm^{-1} modes observed in rhodopsin and isorhodopsin are noteworthy due to their intensity and location. This mode is assigned to the $C_9{=}C_{10}$ stretch in Table VII. Deng and Callender's (1987) force field analysis on rhodopsin yields:

$$Q_R(C_9{=}C_{10}) = 0.28(9 = 10) - 0.20(11 = 12) - 0.11(7 = 8) + \ldots \quad (26)$$

We tentatively assign the enhanced intensity of the 1,599 cm^{-1} band in R and I to counterion perturbation near atom C_{12} enhancing the Raman activity by increasing the excitation induced geometry change. Large changes in atomic charges are predicted to occur upon excitation (Birge and Hubbard, 1980), and our calculations indicate that a counterion located near one end of a delocalized π-system carrying a partial positive charge will enhance a geometry change upon excitation.

We conclude that analysis of the *C=C* stretching modes supports models (such as that shown in Fig. 5) which place the counterion near the center of the polyene chain. Further study is clearly needed to quantify this prediction, but we suggest that more detailed force field studies explicitly including external counterions will support our general predictions.

In summary, we attribute the enhancement of the 1,599 cm^{-1} band in R and I to the presence of a counterion near the center of the polyene chain in the binding site (Figs. 5 *a* and *c*). We attribute the significant protein induced shifts in the fingerprint bands of I and B to conformational distortion of the chromophores. Our models of the isorhodopsin and bathorhodopsin binding sites predict that the chromophores accommodate ~7 kcal mol^{-1} and ~22 kcal mol^{-1} of conformational distortion energy, respectively. These values are relative to rhodopsin, where it is assumed that the chromophore is virtually undistorted relative to the solution conformation (Palings et al., 1987). While our model agrees with a majority of the observations of Palings et al. (1987), we do not agree with the proposal that invariance of the fingerprint bands in R rules out a counterion near the center of the chromophore. For reasons outlined above, we believe the fingerprint bands are relatively insensitive to counterion location. We do agree with Palings et al., that invariance of the fingerprint bands in R is indicative of a relaxed, undistorted chromophore. It is logical that nature would optimize energy storage associated with the primary event by providing a protein binding site that minimized conformational distortion of the absorbing chromophore.

This work was supported in part by grants to R.R.B. from the National Institutes of Health (GM-34549) and the National Science Foundation (CHE-8516155).*Received for publication 20 July 1987 and in final form 9 November 1987*

REFERENCES

Akita, H., S. P. Tanis, M. Adams, V. Balogh-Nair, and K. Nakanishi. 1980. Nonbleachable rhodopsins retaining full natural chromophore. *J. Am. Chem. Soc.* 102:6370–6372.

Asato, A. E., M. Denny, H. Matsumoto, T. Mirzadegan, W. C. Ripka, F. Crescitelli, and R. S. H. Liu. 1986. Study of the shape of the binding site of bovine opsin using 10-substituted retinal isomers. *Biochemistry.* 25:7021–7026.

Baasov, T. and M. Sheves. 1985. Model compounds for the study of spectroscopic properties of visual pigments and bacteriorhodopsin. *J. Am. Chem. Soc.* 107:7524–7533.

Baasov, T., N. Friedman, and M. Sheves. 1987. Factors Affecting the C=N Stretching in Protonated Retinal Schiff Base: a model study for bacteriorhodopsin and visual pigments. *Biochemistry.* 26:3210–3217.

Bagley, K. A., V. Balogh-Nair, A. A. Croteau, G. Dollinger, T. G. Ebrey, L. Eisenstein, M. K. Hong, K. Nakanishi, and J. Vittitow. 1985. Fourier-transform infrared difference spectroscopy of rhodopsin and its photoproducts at low temperature. *Biochemistry.* 24:6055–6071.

Barry, B., and R. A. Mathies. 1987. Raman microscope studies on the primary photochemistry of vertebrate visual pigments with absorption maxima from 430 to 502 nm. *Biochemistry.* 26:59–64.

Becker, R. S., and K. Freedman. 1985. A comprehensive investigation of the mechanism and photophysics of isomerization of a protonated and unprotonated Schiff base of 11-*cis*-retinal. *J. Am. Chem. Soc.* 107:1477–1485.

Bennett, J. A., and R. R. Birge. 1980. Two-photon spectroscopy of

diphenylbutadiene. The nature of lowest-lying $^1Ag^*$-$\pi\pi^*$ state. *J. Chem. Phys.* 73:4234–4246.

Birge, R. R. 1981. Photophysics of light transduction in rhodopsin and bacteriorhodopsin. *Annu. Rev. Biophys. Bioeng.* 10:315–354.

Birge, R. R., J. A. Bennett, L. M. Hubbard, H. L. Fang, B. M. Pierce, D. S. Kliger, and G. E. Leroi. 1982. Two-photon spectroscopy of all-*trans*-retinal. Nature of the low-lying singlet states. *J. Am. Chem. Soc.* 104:2519–2525.

Birge, R. R., and L. M. Hubbard. 1980. Molecular dynamics of *cis-trans* isomerization in rhodopsin. *J. Am. Chem. Soc.* 102:2195–2205.

Birge, R. R., and L. M. Hubbard. 1981. Molecular dynamics of *trans-cis* isomerization in bathorhodopsin. *Biophys. J. 34:517–534.*

Birge, R. R. 1983. One-photon and two-photon excitation spectroscopy. *In* Ultrasensitive Laser Spectroscopy, D. S. Kliger, editor. Academic Press Inc., New York. 109–174.

Birge, R. R., L. P. Murray, B. M. Pierce, H. Akita, V. Balogh-Nair, L. A. Findsen, and K. Nakanishi. 1985. Two-photon spectroscopy of locked 11-*cis*-rhodopsin: evidence for a protonated Schiff base in a neutral binding site. *Proc. Natl. Acad. Sci. USA.* 82:4117–4121.

Birge, R. R., L. P. Murray, R. Zidovetzki, and H. M. Knapp. 1987. Two-photon, ^{13}C and two dimensional ^1H NMR spectroscopic studies of retinyl Schiff bases, protonated Schiff bases, and Schiff base salts: evidence for a protonation induced $\pi\pi^*$ excited state level ordering reversal. *J. Am. Chem. Soc.* 109:2090–2101.

Birge, R. R., and R. H. Callender. 1988. Quantum efficiencies of primary photochemical processes in vertebrate rhodopsin. *In* Biophysical Studies of Retinal Pigments, Proceedings of the Laura Eisenstein Memorial Meeting. K. Nakanishi, editor. In press.

Blatz, P. E., J. H. Mohler, and H. V. Navangal. 1972. Anion-Induced wavelength regulation of absorption maxima of Schiff bases of retinal. *Biochemistry.* 11:848–855.

Callender, R. H., A. Doukas, R. Crouch, and K. Nakanishi. 1976. Molecular flow resonance Raman effect from retinal and rhodopsin. *Biochemistry.* 15:1621–1629.

Cooper, A. 1979a. Energy uptake in the first step of visual excitation. *Nature (Lond.).* 282:531–533.

Cooper, A. 1979b. Energetics of rhodopsin and isorhodopsin. *FEBS (Fed. Eur. Biochem. Soc.) Lett.* 100:382–384.

Crouch, R., V. Purvin, K. Nakanishi, and T. Ebrey. 1975. Isorhodopsin II: Artificial photosensitive pigment formed from 9,13-*dicis* retinal. *Proc. Natl. Acad. Sci. USA.* 72:1538–1542.

Deng, H., and R. H. Callender. 1988. A study of the Schiff base mode in bovine rhodopsin and bathorhodopsin. *Biochemistry.* (in press).

Elinterz, C. M., J. W. Lewis, and D. S. Kliger. 1987. Spectral and kinetic evidence for the existence of two forms of bathorhodopsin. *Proc. Natl. Acad. Sci. USA.* 84:3699–3703.

Eyring, G., and R. Mathies. 1979. Resonance Raman studies of bathorhodopsin: evidence for a protonated Schiff base linkage. *Proc. Natl. Acad. Sci. USA.* 76:33–37.

Eyring, G., B. Curry, A. Broek, J. Lugtenburg, and R. Mathies. 1982. Assignment and interpretation of hydrogen out-of-plane vibrations in the resonance Raman spectra of rhodopsin and bathorhodopsin. *Biochemistry.* 21:384–393.

Gilardi, R. D., I. L. Karle, and J. Karle. 1972. Crystal and molecular structure of 11-*cis* retinal. *Acta Crystallogr., Sec. B.* 28:2605-2612.

Hamanaka, T., T. Mitsui, T. Ashida, and M. Kakudo. 1972. Crystal Structure of all-*trans* retinal. *Acta. Crystallogr. Sect. B. Struct. Crystallogr. Cryst. Chem.* 28:214–222.

Hargrave, P. A., J. H. McDowell, R. J. Feldmann, P. H. Atkinson, J. K. Rao, and P. Argos. 1984. Rhodopsin's protein and carbohydrate structure: selected aspects. *Vision Res.* 24:1487–1499.

Hildebrandt, P., and M. Stockburger. 1984. Role of water in bacteriorhodopsin's chromophore: resonance Raman study. *Biochemistry.* 23:5539–5548.

Hong, K., P. J. Knudsen, and W. L. Hubbell. 1982. Purification of rhodopsin on hydroxyapatite columns, detergent exchange and recombination with phospholipids. *Meth. Enzymol.* 81:144–150.

Honig, B., U. Dinur, K. Nakanishi, V. Balogh-Nair, M. A. Gawinowicz, M. Arnaboldi, and M. G. Motto. 1979a. An external point charge model for wavelength regulation in visual pigments. *J. Am. Chem. Soc.* 101:7084–7086.

Honig, B., T. Ebrey, R. H. Callender, U. Dinur, and M. Ottolenghi. 1979b. Photoisomerization, energy storage, and charge separation: A model for light energy transduction in visual pigments and bacteriorhodopsin. *Proc. Natl. Acad. Sci. USA.* 76:2503–2507.

Honig, B., U. Dinur, R. R. Birge, and T. G. Ebrey. 1980. The isomer dependence of oscillator strengths in retinal and related molecules. Spectroscopic assignments. *J. Am. Chem. Soc.* 102:488–494.

Huppert, D., P. M. Rentzepis, and D. S. Kliger. 1977. Picosecond and nanosecond isomerization kinetics of protonated 11-*cis* retinylidene Schiff bases. *Photochem. Photobiol.* 25:193–197.

Hurley, J. B., T. G. Ebrey, B. Honig, and M. Ottolenghi. 1977. Temperature and wavelength effects of the photochemistry of rhodopsin, isorhodopsin, bacteriorhodopsin and their photoproducts. *Nature (Lond.).* 270:540–542.

Kakitani, H., T. Kakitani, H. Rodman, and B. Honig. 1983. Correlation of vibrational frequencies with absorption maxima in polyenes, rhodopsin, bacteriorhodopsin, and retinal analogues. *J. Phys. Chem.* 87:3620–3628.

Kakitani, H., T. Kakitani, H. Rodman, and B. Honig. 1985. On the mechanism of wavelength regulation in visual pigments. *Photochem. Photobiol.* 41:471–479.

Kliger, D. S., J. S. Horwitz, J. W. Lewis, and C. M. Einterz. 1984. Evidence for a common batho intermediate in the bleaching of rhodopsin and isorhodopsin. *Vision Res.* 24:1465–1470.

Leclercq, J. M., and C. Sandorfy. 1981. On the possibility of protein-chromophore charge transfer in visual pigments. *Photochem. Photobiol.* 33:361–365.

Liu, R. S. H., A. E. Asato, M. Denny, and D. Mead. 1984. The nature of restrictions in the binding site of rhodopsin. A model study. *J. Am. Chem. Soc.* 106:8298–8300.

Liu, R. S. H., and A. E. Asato. 1985. The primary process of vision and the structure of bathorhodopsin: A mechanism for photoisomerization of polyenes. *Proc. Natl. Acad. Sci. USA.* 82:259–263.

Lopez-Garriga, J. J., G. T. Babcock, and J. F. Harrison. 1986a. Increase in the C=N stretching frequency upon complexation of *trans*-retinylidene-n-butylamine with general Lewis acids. *J. Am. Chem. Soc.* 108:7131–7133.

Lopeza-Garriga, J. J., G. T. Babcock, and J. F. Harrison. 1986b. Factors influencing the C=N stretching frequency in neutral and protonated Schiff's bases. *J. Am. Chem. Soc.* 108:7241–7251.

Mao, B., T. G. Ebrey, and R. Crough. 1980. Bathoproducts of rhodopsin, isorhodopsin I and isorhodopsin II. *Biophys. J.* 29:247–256.

Marcus, R. A. 1952. Unimolecular dissociations and free radical recombination reactions. *J. Chem. Phys.* 20:359–364.

Matsumoto, H., and T. Yoshizawa. 1978. Recognition of opsin to the longitudinal length of retinal isomers in the formation of rhodopsin. *Vision Res.* 18:607–609.

Metzler, D. E., and C. M. Harris. 1978. Shapes of spectral bands of visual pigments. *Vision Res.* 18:1417–1420.

Monger, T. G., R. R. Alfano, and R. H. Callender. 1979. Photochemistry of rhodopsin and isorhodopsin investigated on a picosecond timescale. *Biophys. J.* 27:105–116.

Myers, A. G., and R. R. Birge. 1980. The effect of solvent environment on molecular electronic oscillator strengths. *J. Chem. Phys.* 73:5314–5321.

Ottolenghi, M. 1980. The photochemistry of rhodopsins. *Adv. Photochem.* 12:97–200.

Palings, I., J. A. Pardoen, E. van den Berg, C. Winkel, J. Lugtenberg, and R. A. Mathies. 1987. Assignment of fingerprint vibrations in the resonance Raman spectra of rhodopsin, isorhodopsin, and bathorhodopsin: implications for chromophore structure and environment. *Biochemistry.* 26:2544–2556.

Pople, J. A., D. L. Beveridge, and P. A. Dobosh. 1967. Approximate

self-consistent molecular orbital theory. V. Intermediate neglect of differential overlap. *J. Chem. Phys.* 47:2026–2033.

Pratt, D. C., R. Livingston, and K. H. Grellmann. 1964. Flash photolysis of rod particle suspensions. *Photochem. Photobiol.* 3:121–127.

Rafferty, C. N., and H. Shichi, 1981. The Involvement of water at the retinal binding site in rhodopsin and early light-induced intramolecular proton transfer. *Photochem. Photobiol.* 33:229–234.

Rice, O. K. 1962. Effects of quantization and of anharmonicity on the rates of dissociation and association of complex molecules. *J. Phys. Chem.* 65:1588–1596.

Rosenfeld, T., B. Honig, and M. Ottolenghi. 1977. *Cis-trans* isomerization in the photochemistry of vision. *Pure Appl. Chem.* 49:341–351.

Rothschild, K. J., W. A. Cantore, and H. Marrero. 1983. Fourier transform infrared difference spectra of intermediates in rhodopsin bleaching. *Science (Wash. DC).* 219:1333–1335.

Saltiel, J., A. D. Rousseau, and A. J. Sykes. 1972. Temperature and viscosity effects on the decay characteristics of s-trans-1,3-diene triplets. *J. Am. Chem. Soc.* 94:5903–5905.

Sandorfy, C., and D. Vocelle. 1986. The photochemical event in rhodopsin. *Can. J. Chem.* 64:2251–2266.

Sasaki, N., F. Tokunaga, and T. Yoshizawa. 1980a. The formation of two forms of bathorhodopsin and their optical properties. *Photochem. Photobiol.* 32:433–441.

Sasaki, N., F. Tokunaga, and T. Yoshizawa. 1980b. Existence of two forms of bathorhodopsin. *(FEBS Fed. Eur. Biochem. Soc.) Lett.* 114:1–3.

Schaffer, A. M., W. H. Waddell and R. F. Becker. 1974. Visual pigments. IV. Experimental and theoretical investigations of the absorption spectra of retinal Schiff bases and retinals. *J. Am. Chem. Soc.* 96:2063–2068.

Schick, G. A., T. M. Cooper, R. A. Holloway, L. P. Murray, and R. R. Birge. 1987. Energy storage in the primary photochemical events of rhodopsin and isorhodopsin. *Biochemistry.* 26:2556–2562.

Sheves, M., A. Albeck, M. Ottolenghi, P. H. M. Bovee-Geurts, W. J. DeGrip, C. M. Einterz, J. W. Lewis, L. E. Schaecter, and D. S. Kliger. 1986. An artificial visual pigment with restricted C_9-C_{11} motion forms normal photolysis intermediates. *J. Am. Chem. Soc.* 108:6440–6441.

Shichi, H. 1983. Biochemistry of Vision. Academic Press Inc. New York.

Smith, S. O., A. B. Myers, R. A. Mathies, J. A. Pardoen, C. Winkel, E. M. van der Berg, and J. Lugtenberg. 1985. Vibrational analysis of the all-*trans* retinal protonated Schiff base. *Biophys. J.* 47:653–664.

Smith, S. O., M. S. Braiman, A. B. Myers, J. A. Pardoen, J. M. L. Courtin, C. Winkel, J. Lugtenberg, and R. A. Mathies. 1987. Vibrational analysis of the all-*trans* retinal chromophore in light-adapted bacteriorhodopsin. *J. Am. Chem. Soc.* 109:3108–3125.

Sperling, W., 1972. Conformations of 11-*cis* retinal. *In* Biochemistry and Physiology of Visual Pigments. editor. H. Langer. Springer-Verlag, New York Inc., NY. pp 19–289.

Stryer, L. 1986. Cyclic GMP cascade of vision. *Annu. Rev. Neurosci.* 9:87–119.

Suzuki, T., and R. H. Callender. 1981. Primary photochemistry and photoisomerization of retinal at 77°K in cattle and squid rhodopsins. *Biophys. J.* 34:261–265.

Waddell, W. H., and K. Chihara. 1981. Activation barriers for the *trans* → *cis* photoisomerization of all-*trans* retinal. *J. Am. Chem. Soc.* 103:7389–7390.

Wald, G., and P. K. Brown. 1953. Molar extinction of rhodopsin. *J. Gen. Physiol.* 37:189–200.

Warshel, A., and N. Barboy. 1982. Energy storage and reaction pathways in the first step of the vision process. *J. Am. Chem. Soc.* 104:1469–1676.

Yoshizawa, T. 1972. The behavior of visual pigments at low temperatures. Handbook of Sensory Physiology. VII. 1:146–179.

Yoshizawa, T., and G. Wald. 1963. Pre-lumirhodopsin and the bleaching of visual pigments. *Nature (Lond.).* 197:1279–1286.